

Elsevier Editorial System(tm) for
Atmospheric Environment
Manuscript Draft

Manuscript Number: ATMENV-D-16-00493R2

Title: Abiotic and seasonal control of soil-produced CO₂ efflux in karstic ecosystems located in Oceanic and Mediterranean climates

Article Type: Research Paper

Keywords: Vadose Zone, CO₂ exchange, $\delta^{13}\text{C}\text{O}_2$, Climatic control, Soil CO₂ diffusion

Corresponding Author: Dr. Elena Garcia-Anton,

Corresponding Author's Institution: Department of Geology, National Museum of Natural Sciences (MNCN-CSIC), 28006 Madrid, Spain

First Author: Elena Garcia-Anton

Order of Authors: Elena Garcia-Anton; Soledad Cuezva; Angel Fernandez Cortes; Miriam Alvarez-Gallego; Concepcion Pla; David Benavente; Juan Carlos Cañaveras; Sergio Sanchez-Morall

Abstract: This study characterizes the processes involved in seasonal CO₂ exchange between soils and shallow underground systems and explores the contribution of the different biotic and abiotic sources as a function of changing weather conditions. We spatially and temporally investigated five karstic caves across the Iberian Peninsula, which presented different microclimatic, geologic and geomorphologic features. The locations present Mediterranean and Oceanic climates. Spot air sampling of CO₂ (g) and $\delta^{13}\text{C}\text{O}_2$ in the caves, soils and outside atmospheric air was periodically conducted. The isotopic ratio of the source contribution enhancing the CO₂ concentration was calculated using the Keeling model. We compared the isotopic ratio of the source in the soil ($\delta^{13}\text{C}\text{s-soil}$) with that in the soil-underground system ($\delta^{13}\text{C}\text{s-system}$). Although the studied field sites have different features, we found common seasonal trends in their values, which suggests a climatic control over the soil air CO₂ and the $\delta^{13}\text{C}\text{O}_2$ of the sources of CO₂ in the soil ($\delta^{13}\text{C}\text{s-soil}$) and the system ($\delta^{13}\text{C}\text{s-system}$). The roots respiration and soil organic matter degradation are the main source of CO₂ in underground environments, and the inlet of the gas is mainly driven by diffusion and advection. Drier and warmer conditions enhance soil-exterior CO₂ interchange, reducing the CO₂ concentration and increasing the $\delta^{13}\text{C}\text{O}_2$ of the soil air. Moreover, the isotopic ratio of the source of CO₂ in both the soil and the system tends to heavier values throughout the dry and warm season. We conclude that seasonal variations of soil CO₂ concentration and its ¹³C/¹²C isotopic ratio are mainly regulated by thermo-hygrometric conditions. In cold and wet seasons, the increase of soil moisture reduces soil diffusivity and allows the storage of CO₂ in the subsoil. During dry and warm seasons, the evaporation of soil water favours diffusive and advective transport of soil-derived CO₂ to the atmosphere. The soil CO₂ diffusion is enough important during this season to modify the isotopic ratio of soil produced CO₂ (3-6% heavier). Drought induces release of CO₂ with an isotopic ratio heavier than produced by organic sources. Consequently, climatic conditions drive abiotic processes that

turn regulate a seasonal storage of soil-produced CO₂ within soil and underground systems. The results here obtained imply that abiotic emissions of soil-produced CO₂ must be an inherent consequence of droughts, which intensification has been forecasted at global scale in the next 100 years.

Abiotic and seasonal control of soil-produced CO₂ efflux in karstic ecosystems located in Oceanic and Mediterranean climates

Elena Garcia-Anton¹, Soledad Cuezva^{1,2}, Angel Fernandez-Cortes³, Miriam Alvarez-Gallego¹, Concepcion Pla⁴, David Benavente⁵, Juan Carlos Cañaveras⁵, Sergio Sanchez-Moral¹

¹ Department of Geology, National Museum of Natural Sciences (MNCN-CSIC), 28006 Madrid, Spain. elena.garcia@mncn.csic.es, scuezva@mncn.csic.es, mag@mncn.csic.es, ssmilk@mncn.csic.es

² Geomnía Natural Resources SLNE, 28003 Madrid, Spain.

³ Department of Biology and Geology, University of Almería, 04120 Almería, Spain. acortes@ual.es

⁴ Department of Civil Engineering, University of Alicante, San Vicente del Raspeig, 03690 Alicante, Spain. c.pla@ua.es

⁵ Department of Environment and Earth Sciences, University of Alicante, San Vicente del Raspeig, 03690 Alicante, Spain. david.benavente@ua.es, jc.canaveras@ua.es

Abstract

1 This study characterizes the processes involved in seasonal CO₂ exchange between soils and
2 shallow underground systems and explores the contribution of the different biotic and abiotic
3 sources as a function of changing weather conditions. We spatially and temporally investigated
4 five karstic caves across the Iberian Peninsula, which presented different microclimatic,
5 geologic and geomorphologic features. The locations present Mediterranean and Oceanic
6 climates. Spot air sampling of CO₂ (g) and δ¹³CO₂ in the caves, soils and outside atmospheric air
7 was periodically conducted. The isotopic ratio of the source contribution enhancing the CO₂
8 concentration was calculated using the Keeling model. We compared the isotopic ratio of the
9 source in the soil (δ¹³C_s-soil) with that in the soil-underground system (δ¹³C_s-system).
10 Although the studied field sites have different features, we found common seasonal trends in
11 their values, which suggests a climatic control over the soil air CO₂ and the δ¹³CO₂ of the
12 sources of CO₂ in the soil (δ¹³C_s-soil) and the system (δ¹³C_s-system). The roots respiration and
13 soil organic matter degradation are the main source of CO₂ in underground environments, and
14 the inlet of the gas is mainly driven by diffusion and advection. Drier and warmer conditions
15 enhance soil-exterior CO₂ interchange, reducing the CO₂ concentration and increasing the
16 δ¹³CO₂ of the soil air. Moreover, the isotopic ratio of the source of CO₂ in both the soil and the
17 system tends to heavier values throughout the dry and warm season.

18 We conclude that seasonal variations of soil CO₂ concentration and its ¹³C/¹²C isotopic ratio are
19 mainly regulated by thermo-hygrometric conditions. In cold and wet seasons, the increase of
20 soil moisture reduces soil diffusivity and allows the storage of CO₂ in the subsoil. During dry
21 and warm seasons, the evaporation of soil water favours diffusive and advective transport of
22 soil-derived CO₂ to the atmosphere. The soil CO₂ diffusion is enough important during this
23 season to modify the isotopic ratio of soil produced CO₂ (3-6‰ heavier). Drought induces
24 release of CO₂ with an isotopic ratio heavier than produced by organic sources. Consequently,
25 climatic conditions drive abiotic processes that turn regulate a seasonal storage of soil-
26 produced CO₂ within soil and underground systems. The results here obtained imply that
27 abiotic emissions of soil-produced CO₂ must be an inherent consequence of droughts, which
28 intensification has been forecasted at global scale in the next 100 years.

29 *Keywords:* Vadose Zone, CO₂ exchange, δ¹³CO₂, Climatic control, Soil CO₂ diffusion

30 **1 Introduction**

31 Climate change is expected to modify current climate producing not only a progressive global
32 warming but also changes on the frequency, the severity and the nature of the climatic
33 extreme events. Current climate models forecast a global intensification of heavy precipitation
34 events, heat extremes and longer and stronger droughts (Ciais et al., 2013). This may produce
35 substantial changes in the ecosystems affecting therefore to carbon cycling and its feedbacks
36 to the climate system. There are still many uncertainties related to the processes controlling
37 ecosystem carbon fluxes. Thus, responses of the environment to climate changes have not yet
38 been completely determined in terms of time, direction or intensity (Frank et al., 2015).

39 Diverse climate-dependent processes occurring on different timescales (i.e., from hours to
40 millions of years) are involved in ecosystems carbon cycling (Berner, 2003). Among them,
41 carbonate weathering and underground CO₂ storage are abiotic processes that are considered
42 significant parts of the terrestrial flux of carbon at short time scales (hourly, daily and annually

43 (Liu and Zhao, 2000; Mörner and Etiope, 2002; Kowalski et al., 2008; Gilfillan et al., 2009;
44 Serrano-Ortiz et al., 2010; Roland et al., 2013; Fernandez-Cortes et al., 2015a)). Part of these
45 carbon fluxes takes place in the subsoil vadose zone in which aqueous and gaseous
46 transference processes of CO₂ between the underground environment and the overlying soil
47 are regulated essentially by the temperature and water content of the soil-rock layer (Cuevza
48 et al., 2011; Pla et al., 2017a).

49 Subsurface caves in the vadose zone commonly present high concentration of CO₂ compared
50 to outdoor air. The main source of the CO₂ in the caves results from the organic activity taking
51 place in the overlying soil (Baldini et al., 2006; Genty et al., 2008, Fig. 1) and/or the vadose
52 zone (Noronha et al., 2015; Matthey et al., 2016). Soil CO₂ efflux is the largest terrestrial flux of
53 CO₂, known as soil respiration (Ryan and Law, 2005; Jassal et al., 2007). Moreover, lately
54 studies have identified an important source of CO₂ in caves in the decay of soil organic matter
55 washed down into the unsaturated zone (Matthey et al., 2016). The transfer of organic-derived
56 CO₂ towards less concentrated zones and throughout the system of air-filled pores, cracks and
57 voids in bedrock is favoured by the diffusive mechanism (mass transport process) triggered as
58 a response to the concentration gradient (Christoforou et al., 1996; Bourges et al., 2001;
59 Breecker et al., 2012; Garcia-Anton et al., 2014a). Additionally, advection (bulk air movement)
60 has been observed to be an important mechanism of CO₂ transport throughout some
61 underground environments (Frisia et al., 2011; Fernandez-Cortes et al. 2015a; Matthey et al.,
62 2016). Organic derived CO₂ also can reach the cave by geochemical dissolution in infiltrating
63 water and afterward degassing in the underground environment (Fig. 1). This process is linked
64 to speleothems formation. Nevertheless, several important studies concluded that CO₂ supply
65 by dripping waters in caves is relatively low compared to the soil-derived CO₂ inlet in gaseous
66 phase (Baldini et al., 2006; Frisia et al., 2011; Breecker et al., 2012).

67 The CO₂ stored in caves commonly presents variations strongly driven by ventilation (advective
68 air movement) due to the inflow of less concentrated exterior air and the simultaneous
69 outflow of the underground air (Fernandez-Cortes et al., 2009; Frisia et al., 2011; Garcia-Anton
70 et al., 2014a, Fig. 1). Ventilation episodes are regulated by synoptic weather conditions
71 (Bourges et al., 2001; Matthey et al., 2010; Fernandez-Cortes et al., 2011; Fernandez-Cortes et al
72 2015a, among others). Rainfall and the relative humidity of air regulate the water content in
73 soil and host rock porous media that play important roles in regulating the gas exchange
74 between the underground environment and the surface (Cuezva et al., 2011; Fernandez-Cortes
75 et al., 2013). Air density contrasts (controlled by temperature gradient between the cave air
76 and the atmosphere) and cave geometry determine the advective movement of air that
77 produces the cave ventilation (Fernandez-Cortes et al., 2009; Faimon et al., 2012; Sanchez-
78 Cañete et al., 2013; James et al., 2015). Interior temperature of caves is in general very stable
79 compared to the exterior air due to the characteristic low thermal conductivity of rocks. This
80 generates significant interior-exterior temperature contrasts that trigger ventilation and air
81 exchange processes. On the other hand, caves morphology determines the inner-outer air
82 masses altitudinal relationship, which in most of the cases determines caves ventilation
83 patterns throughout the year (Faimon et al., 2012). Ventilation of caves releases the stored
84 underground air that can influence seasonal and daily CO₂ fluxes between soil-subsoil and the
85 atmosphere at local scale (Kowalski et al., 2008; Sanchez-Cañete et al., 2011; Hamerlynck et
86 al., 2013; Chen et al., 2014; Wang et al., 2014). Discriminating the biogeochemical processes
87 occurring through the rock and soil involving CO₂ is key to understanding the surface-
88 atmosphere exchange of CO₂ in terrestrial ecosystems. The $\delta^{13}\text{C}$ of CO₂ ($\delta^{13}\text{CO}_2$) in air has been
89 traditionally studied to identify the characteristic $\delta^{13}\text{CO}_2$ of ecosystem respiration and the
90 contribution of different biotic or abiotic sources (Yakir and Sternberg, 2000; Pataki et al.,
91 2003; Hemming et al., 2005). The isotopic ratio characterizes the chemical changes undergone
92 by the gas, introducing identifiers for the source of production and transport mechanisms

93 (Maseyk et al., 2009; Kayler et al., 2010; Moyes et al., 2010; Bowling and Massman 2011;
94 Shanhun et al., 2012; Garcia-Anton et al., 2014a). In studies carried out in natural
95 environments, the $\delta^{13}\text{C}$ of the source contributing to enhance the CO_2 concentration in air
96 can be easily obtained by mass-balance estimations such as the Keeling approach (Keeling,
97 1958; Keeling, 1961). Traditionally, the Keeling plot has been used to identify the $\delta^{13}\text{C}$ of a
98 single source component contributing to the ecosystem. However, in this work, we applied the
99 Keeling plot to study the interaction between three components of a karst system: exterior
100 atmosphere, soil air and subsurface stored air. The data treatment applied highlights the
101 differences between the isotopic ratio characterizing the soil contribution and the isotopic
102 ratio corresponding to the combination of the soil and the underground system contribution.

103 The aim of the present research is to characterize biotic and abiotic processes involved in CO_2
104 exchange in the underground-soil-atmosphere system at the seasonal/annual scale. We
105 examine the role of the vadose zone influencing ecosystem CO_2 fluxes as function of climate
106 changes. We spatially and temporally investigated five karstic locations across the Iberian
107 Peninsula with different geologic and geomorphologic features located at Oceanic and
108 Mediterranean climates. The different locations gave us a broad view of the response of the
109 systems to a range of conditions: from extremely hot and dry (Mediterranean climate
110 summers) to temperate and humid (Oceanic climate). We focused our study on the variability
111 of the isotopic signal $\delta^{13}\text{C}$ of the source of CO_2 . Spot air sampling of CO_2 (g) and $\delta^{13}\text{C}$ of the
112 three major air masses involved (cave, soil and outside atmosphere) was periodically
113 conducted (monthly and bimonthly). The main environmental conditions at the surface
114 (temperature, relative humidity and rainfall) and inside the cave atmosphere (temperature,
115 relative humidity and gases concentration in the air) were continuously measured and
116 registered by monitoring systems during the sampling periods at each field site.

117 **2. Sites, materials and methodology**

118 2.1 Field sites

119 The studied sites are different caves located in the Iberian Peninsula (Fig. 2) that present
120 different geologic, morphologic and climatic conditions. Different features of the studied caves
121 are suitable to both identify common processes occurring in underground environments and
122 distinguish them from local effects. Table 1 synthesizes relevant available information about
123 the field sites.

124 2.1.1 Altamira

125 Altamira cave is a shallow vadose karst cavity located in a hill 161 m.a.s.l. at a depth of 322 m
126 (8 m on average) below the surface (Fig. 3). The cavity has a single entrance in a
127 topographically higher position (152 m.a.s.l.) and includes several main rooms that have a
128 downward trend from the outside access to the deepest part of the cave. The host rock in the
129 Altamira Cave is a thin to medium, parallel bedded, Cenomanian (Upper Cretaceous) limestone
130 succession from 13.5 to 15 m thick.

131 Altamira cave is located in an Oceanic or specifically Warm temperate climate, fully humid with
132 a temperate summer (Cfb climate type, Köppen-Geiger Classification slightly modified, AEMET-
133 IM, 2011, Fig. 2, Table 1). The annual precipitation is approximately 1400 mm and the mean
134 annual temperature and relative humidity are approximately 14 °C and 85%, respectively.

135 The cave was defined in Cuezva et al., (2009) as a stable environment, with high thermo-
136 hygrometric stability throughout the year (ranges of monthly average temperatures: 13.38-
137 14.56 °C, Garcia-Anton et al., 2014b) and a low energy exchange with the surface. Relatively
138 high levels of air CO₂ are registered during winter and lowest values during summer (from June
139 to October), due to the most effective cave ventilation in this warmer and drier period (ranges
140 CO₂ concentrations: 677-5576 ppm, Garcia-Anton et al., 2014b). The characteristic ventilation
141 pattern in this cave contrasts to the classical models (Mangin and Andrieux, 1988), in which

142 downward caves with a unique entrance in its upmost part are expected to present their
143 ventilation stage during the winter (according to the inner-outer density/temperature
144 gradient). Therefore, the cave must have unknown connections to the surface that allow active
145 chimney-effect air movements during the summer. These connections have been identified in
146 previous studies (Garcia-Anton et al., 2014a) and located in the lowest part of the cave (Well
147 Hall, Fig. 3).

148 Water supply in this cave is relatively low and restricted to seepage waters. Maximum
149 infiltration rates occur during autumn and winter, and occasionally during spring, whereas
150 practically null percolation rates characterize the summer season (Cuezva, 2008).
151 Consequently, speleothem development is scarce in this cave.

152 2.1.2 Castañar de Ibor

153 Castañar de Ibor cave is hosted in Neoproterozoic rocks that form the core of the Ibor
154 Anticline. These rocks are shales and greywackes with interbedded dolostones and magnesites
155 (Alonso-Zarza et al., 2011). The cave was developed by the dissolution of the dolomitic beds.
156 Besides, the extensive weathering of the shales and greywackes favours collapses, which
157 created and enlarged the cave. Castañar de Ibor cave exhibits a maze pattern with a
158 labyrinthine distribution of galleries that indicates a strong structural and lithological control
159 on its formation (Fig. 4). The cave entrance is currently a vertical access, 9 m long over an area
160 of 1.5 m², with a quasi-hermetic trap door installed at the entrance.

161 The geographical area is characterized by a Mediterranean or specifically Warm temperate
162 climate with a dry and hot summer (Csa climate type, Köppen-Geiger Classification slightly
163 modified, AEMET-IM, 2011, Fig. 2, Table 1). The annual precipitation is relatively low (slightly
164 above 500 mm/year) with long periods of drought and maximum rainfall in autumn. Mean
165 annual temperature is 15.5°C.

166 The Castañar de Ibor cave is a low energy and quite isolated cave with very high thermal
167 stability throughout the annual cycle under natural conditions (monthly- averaged
168 temperatures and CO₂ concentrations range 16.93-16.96 °C and 3364-3866 ppm, respectively,
169 Fernandez-Cortes et al., 2011). The high stability on the climate conditions of the Castañar de
170 Ibor cave is due to the scarce interchange with the exterior air, mainly driven by natural
171 barometric fluxes (Fernandez-Cortes et al., 2011). This type of microclimate is characteristic of
172 cavities relatively well connected with exterior, with a single small entrance located above the
173 cave (Choppy, 1982).

174 Water inlet in the cave from exterior is restricted to slow infiltration that feed three small lakes
175 (Fernandez-Cortes et al., 2010; Garcia-Guinea et al., 2013). This cave is especially remarkable
176 by the quantity and variety of speleothems. Massive speleothems are associated with main
177 fractures and bedding planes, while branching and fibrous, mostly aragonite, speleothems are
178 related with capillary seepage or drip water (Alonso-Zarza et al., 2011).

179 2.1.3 Ojo Guareña

180 Ojo Guareña karst system is hosted in Upper Cretaceous limestones and dolomitic limestones
181 (Camacho et al., 2006). In this geographic area, the climate is Oceanic or specifically Warm
182 temperate climate, fully humid with a temperate summer (Cfb climate type, Köppen-Geiger
183 Classification slightly modified, AEMET-IM, 2011, Fig. 2, Table 1). The annual mean
184 precipitation is approximately 640 mm, and the average annual temperature is 11.9 °C
185 (Fernandez-Cortes et al., 2015b).

186 The Ojo Guareña cave system, one of the longest cave systems in Europe with over 100 km of
187 development, is distributed over several overlapping levels composed of passages up to 10 m
188 high and 20 m wide with 3 main entrances and several other minor cavities. In the sinkhole
189 plain, we can find several entrances to the subterranean karst system, such as the Palomera
190 doline and Dolencias sinkhole. Present study was conducted in a sector 3 km in length. This

191 sector represents only 2 % of the entire subterranean system (Fig. 5, Grupo Espeleológico
192 Edelweiss, 1986; Camacho et al., 2006).

193 Previous studies have described Ojo Guareña as an underground environment with strong
194 rapid (daily) variations in temperature and trace gases concentration (CO₂ and ²²²Rn). This
195 indicates a high-energy exchange between the exterior atmosphere and the cavity (during an
196 annual cycle cave temperatures and CO₂ concentrations ranges are 2-11°C and 400-4500 ppm,
197 respectively, Fernandez-Cortes et al., 2015a). This cave presents seasonally reversing, chimney-
198 effect winds, which is typical of caves with multiple connections with exterior atmosphere
199 (Mangin and Andrieux, 1988).

200 Ojo guareña cave system is developed by a sinking stream that inundates the most of the
201 gallery during the rainfall periods (Fernandez-Cortes et al., 2015a). It constitutes the main
202 water supply from exterior. The inflow rate of water via the Ojo Guareña sinking Stream ranges
203 from 0.1 m³ s⁻¹ during the dry season to 0.65 m³ s⁻¹ in winter and spring (Grupo Espeleológico
204 Edelweiss Grupo Espeleológico Edelweiss 1986). In general, chemical dissolution dominates
205 over carbonate precipitation. The more isolated spots inside the cave, with very low energy
206 and matter exchange, presents active speleothems, as Museo de Cera chamber (Fig. 5).

207 2.1.4 Rull

208 Rull cave is located in massive Miocene conglomerates, with considerable textural and
209 petrophysical complexity, which were deposited on Cretaceous limestones (Pla et al., 2016 and
210 2017a, b). The cave consists in a single chamber with relatively small dimensions compared to
211 the other study sites surveyed in the study (Fig. 6).

212 The geographical area of Rull cave is characterized by a Mediterranean or specifically Warm
213 temperate climate with a dry and hot summer (Csa climate type, Köppen-Geiger Classification

214 slightly modified, AEMET-IM, 2011, Fig. 2, Table 1). Mean annual temperature in Rull cave area
215 is around 16°C and total annual precipitation is approximately 300 mm.

216 Rull cave environment has a high thermo-hygrometric stability throughout an annual cycle.
217 Mean temperature inside the cavity is of 16.4 °C and the thermal amplitude is lower than 0.5
218 °C. The gaseous regimen in the indoor atmosphere is characterized by annual cycles with two
219 main stages. Throughout the outgassing [stage](#), ventilation (temperature-driven [airflow](#)) is
220 responsible for the gaseous removal from the cavity when the cave temperature is higher than
221 the outdoor temperature. During the warmest season, when outdoor temperature is higher
222 than the cave temperature, the cavity suffers an isolation stage; the gaseous interchange is
223 limited and, as consequence, the gaseous concentration increases sharply (Pla et al., 2016).
224 This pattern is typical of caves with a downward tendency with a unique entrance located on
225 the top (such as the Rull cave, Mangin and Andrieux, 1988). Colder and heavier air inflows in
226 the cavity expelling the inner warmer and lighter air. Throughout an annual cycle, in Rull cave,
227 CO₂ air concentrations normally range from 800 to 4000 ppm.

228 [The water infiltration through dripping points is the main process of water recharge in Rull](#)
229 [cave. There are not any evidences of water runoff along the cave passages. The cave presents](#)
230 [low seeping rates during an annual cycle with maximum dripping during winter \(Pla, 2017b\).](#)
231 [Torrential rainfalls primarily control dripping water activation. Inside the cave, there is a large](#)
232 [quantity of speleothems \(stalactites, stalagmites, flowstones etc.\) with diverse mineralogy](#)
233 [although prevailing calcite.](#)

234 2.1.5 El Sidron

235 The karstic site of El Sidron is found in the so-called “Surco Oviedo-Infiesto” a strip of
236 Mesozoic and Cenozoic sediments limited by Paleozoic relief to the north and south. The cavity
237 is a pression tube of 600 m long, with a central stretch of 200 m oriented nearly west east. This

238 tube shows on its southern bank transverse galleries in a NE–SW to N–S direction, generally of
239 a restricted nature (Fig. 7, Rosas et al., 2006).

240 El Sidron cave is influenced by an Oceanic or specifically Warm temperate climate, fully humid
241 with a temperate summer (Cfb climate type of the Köppen-Geiger Classification slightly
242 modified, AEMET-IM, 2011, Fig. 2, Table 1). Mean annual temperature is approximately 13.1 °C
243 and annual precipitation is around 1300 mm. Own data (not published) show a stable interior
244 temperature throughout the year around 12 °C and relatively high ventilation rate
245 characteristic of caves with multiple connections with the surface (Mangin and Andrieux,
246 1988).

247 El Sidron cave is part of a karstic valley developed by a stream feed by external runoff and
248 infiltration waters. It disappears in the eastern part of the valley in a sinkhole that descends to
249 lower karstic levels (Peña et al., 2011). The main gallery of El Sidron cave is seasonally flooded
250 and subterranean river is active throughout year with high water flow during the rainy
251 seasons. Speleothems can be observed in the cave, mainly flowstones, though chemical
252 dissolution dominates over carbonate precipitation.

253 2.1 Monitoring systems

254 Surface stations recorded climate parameter variability outside the caves: temperature,
255 relative humidity and rainfall amount. The Altamira and Castañar de Ibor caves had an
256 additional monitoring system continuously measuring and registering the temperature and
257 humidity in the soil zone (at 5 cm depth in Altamira and at 5, 30 and 50 cm depth in Castañar
258 de Ibor). Inner climatic conditions (temperature, relative humidity, among others) were
259 monitored in the Altamira, Castañar de Ibor, Ojo Guareña and Rull caves jointly with the radon-
260 222 (²²²Rn) concentration in the underground air as a tracer of ventilation (Lario et al., 2006;
261 Richon et al., 2011). In the El Sidron cave, the exterior and inner temperature and relative
262 humidity of the air were also registered. Altamira, Castañar de Ibor and Rull caves monitoring

263 systems were fed by electric current while El Sidron and Ojo Guareña systems were battery
264 powered.

265 Rainfall amount was registered in Altamira, Castañar de Ibor, Ojo Guareña and Rull caves by
266 RG2-M pluviometers (Onset Computer Corporation, Bourne, MA, USA, resolution 0.2 mm). Air
267 temperature and relative humidity were monitored outside Altamira and El Sidron and inside
268 El Sidron and Ojo Guareña caves by HOBO U23 Pro v2 probes (Onset Computer Corporation,
269 Bourne, MA, USA, accuracy ± 0.2 °C and $\pm 2.5\%$, respectively). The soil water volumetric content
270 was measured in Altamira and Castañar de Ibor by ECHO EC-10 probes (Decagon Devices,
271 Pullman, WA, U.S.A., accuracy 1-2%). Inner air temperature and relative humidity in Castañar
272 de Ibor and Rull caves were surveyed by Rotronic probes HygroClip S3 with a Pt100 1/10 DIN
273 thermometer and a humidity sensor (accuracy $\pm 0.6\%$). The ^{222}Rn concentration of cave air was
274 continuously registered in Altamira, Castañar de Ibor, Ojo Guareña and Rull caves using Radim
275 5WP monitors (GT-Analytic KG, Lambesc, France, accuracy ± 0.3 (imp·Bq/h·m³)).

276 In Altamira cave, exterior soil temperature was tested by a TMC20-HD probe (Onset Computer
277 Corporation, Bourne, MA, USA, accuracy ± 0.5 °C). Inside of the cave, air temperature and
278 humidity were surveyed by a Pt100 1/10 DIN sensor (accuracy ± 0.03 °C) and a Hygroclip 1/5
279 DIN (Rotronic, Bassersdorf, Switzerland, accuracy $\pm 0.8\%$), respectively. In Castañar de Ibor,
280 exterior air temperature and relative humidity were tested by a S-THB Sensor (Onset
281 Computer Corporation, Bourne, MA, USA, accuracy ± 0.2 °C and $\pm 2.5\%$, respectively). Exterior
282 soil temperature was controlled by a S-TMB-M006 sensor (Onset Computer Corporation,
283 Bourne, MA, USA, accuracy ± 0.2 °C). In Ojo Guareña cave, the exterior air temperature and
284 relative humidity were measured with a HOBO-U21 data logger (Onset Computer Corporation,
285 Bourne, MA, USA, accuracy ± 0.01 °C and $\pm 0.03\%$ RH). Outside of the Rull cave, a weather
286 station with an independent data logger (HOBO U12, Onset Computer Corporation, Bourne,

287 MA, USA) recorded the air temperature (accuracy ± 0.2 °C) and relative humidity (accuracy
288 $\pm 3.5\%$).

289 Further details related to the monitoring systems for the Altamira, Castañar de Ibor, Ojo
290 Guareña and Rull caves can be found in previous articles (Fernandez-Cortes et al., 2011;
291 Garcia-Anton et al., 2014a; Fernandez-Cortes et al., 2015a; Pla et al., 2016).

292 2.2 Collection and analysis of air samples

293 A specific sampling and analysis program was designed and implemented to obtain data on
294 CO₂ (g) and $\delta^{13}\text{CO}_2$ inside of the caves, the soil above the caves and the exterior atmosphere in
295 their emplacements. Field campaigns (1-2 days long) were periodically carried out for
296 collecting air samples in a spatially-distributed network of points in the caves, the soils and the
297 exterior. Sampling work was conducted in each single site during a complete annual cycle. Soil
298 air was extracted using an iron tube nailed to the ground by means of a micro-diaphragm gas
299 pump (KNF Neuberger, Freiburg, Germany) at 3.1 l/min at atmospheric pressure. Cave air and
300 exterior air were sampled using a low-flow pump and the resulting air aliquots were saved in 1
301 l Tedlar bags with lock valves. [The total number of samples collected at the different sites was](#)
302 [190, 265 and 482 for exterior, soil and cave air respectively.](#) Bag samples were analysed no
303 later than 48 h after sampling using a Picarro G2101-i analyser. The system uses *cavity ring-*
304 *down spectroscopy (CRDS)* to identify and quantify the compounds contained in the analysed
305 air (Crosson, 2008). The analyser measures the isotopologues of the carbon dioxide ($^{12}\text{CO}_2$ and
306 $^{13}\text{CO}_2$) and automatically calculates the $\delta^{13}\text{CO}_2$. The device measurement precisions are 200
307 ppb and 10 ppb for $^{12}\text{CO}_2$ and $^{13}\text{CO}_2$, respectively. The resulting accuracy is 0.3‰ for $\delta^{13}\text{CO}_2$
308 after 5 minutes of analysis.

309 [Three in-house standards with certified gas mixtures and known CO₂ concentration \(7000 ppm,](#)
310 [400 ppm and zero-CO₂, supplied by PRAXAIR Spain in high-pressure gas cylinders for this study\)](#)
311 [were run regularly at the beginning and at the end of each day/session of analyses to verify the](#)

312 proper functioning of the Picarro G2101-I analyser. Further details about the methodological
313 procedures and quality results can be found in Fernandez-Cortes et al. (2015b). In addition,
314 both in-house standards and air samples were also subjected to quality control by comparing
315 the results obtained with the Picarro G2101-i analyser with duplicated bags collected, in situ
316 (on field) and from cylinders, and subsequently analyzed independently in the greenhouse gas
317 laboratory at Royal Holloway University of London (RHUL). CH₄ and CO₂ mole fractions of these
318 duplicated samples were measured in the RHUL lab with a Picarro G1301 CRDS analyzer and
319 the $\delta^{13}\text{CO}_2$ was measured in triplicate by continuous flow gas chromatography isotope ratio
320 mass spectrometry (CF GC-IRMS) using a GV Instruments TraceGas – Isoprime system (Fisher et
321 al., 2006). Both equipments were regularly calibrated against the NOAA (National Oceanic and
322 Atmospheric Administration) using internal secondary standard tanks gas and a NOAA
323 standard cylinder. The repeatability obtainable with CF GC-IRMS is 0.03 ‰ for ¹³CO₂ for ten
324 consecutive analyses of a standard tank (Fisher et al., 2006).
325 These internal and inter-comparison procedures periodically confirmed that the performance
326 specifications regarding CO₂ analyses via our CRDS analyzer were met.

327

328 2.3 Data analysis

329 The CO₂/δ¹³CO₂ results of the samples analysis were studied using the Keeling approach. The
330 Keeling plot incorporates the assumption that each data point represents a mixture of two
331 end-member gases. The first is generally considered the background atmosphere and the
332 second end-member is assumed to be pure CO₂ (CO₂ source) that has been added to
333 atmospheric air to produce the composition of the observed point. The isotopic composition of
334 source CO₂ (δ¹³CO₂) is estimated with the Keeling plot by extrapolating the straight line joining
335 the atmospheric end-member to the data point under consideration, as far as its intersection

336 with the $\delta^{13}\text{C}$ axis. This method is widely used to characterize the $\delta^{13}\text{CO}_2$ of ecosystem
 337 respiration (Keeling, 1958; Keeling, 1961; Yakir and Sternberg, 2000; Pataki et al., 2003), and it
 338 has recently been used to determine the source of the high concentration of CO_2 measured in
 339 caves (Spotl et al., 2005; Matthey et al., 2010; Frisia et al., 2011).

340 The Keeling approach is based on a simplified two-end member model: the isotopic **ratio** of the
 341 CO_2 concentration in the studied air mass (a) results from the proportional mixing of the
 342 $\delta^{13}\text{CO}_2$ of a background concentration of CO_2 (b) and the $\delta^{13}\text{CO}_2$ of the CO_2 added from
 343 unknown sources:

$$344 \quad [\text{CO}_2]_a \cdot \delta^{13}C_a = [\text{CO}_2]_b \cdot \delta^{13}C_b + [\text{CO}_2]_s \cdot \delta^{13}C_s \quad (1)$$

345 The background concentration represents the CO_2 of the clean troposphere characterized by a
 346 present-day isotopic **ratio** of near -8‰ (Vaughn et al., 2010; Bowling et al., 2014). The method
 347 provides the value of the source without any information about the concentration or the
 348 isotopic **ratio** of the background component (none of them are spatially or temporally constant
 349 variables). The isotopic $^{13}\text{C}/^{12}\text{C}$ ratio of added CO_2 is easily obtained as the intercept of the
 350 fitted line of the $[1/\text{CO}_2, \delta^{13}\text{CO}_2]$ points resulting from the analysis of the air samples. By
 351 assuming:

$$352 \quad [\text{CO}_2]_a = [\text{CO}_2]_b + [\text{CO}_2]_s \quad (2)$$

353 and by combining equations 1 and 2:

$$354 \quad \delta^{13}C_a = [\text{CO}_2]_b \cdot (\delta^{13}C_b - \delta^{13}C_s) \cdot (1/[\text{CO}_2]_a) + \delta^{13}C_s \quad (3)$$

355 When more than two end-members are present in the mixture of air, then the Keeling plot will
 356 give also the $\delta^{13}\text{C}$ of the pure CO_2 (CO_2 source) that would have to be added to atmospheric air
 357 to produce the composition for the data point under consideration. This is of course only an
 358 apparent composition, and does not correspond to a real source of CO_2 if there are other

359 processes occurring, for [example](#), diffusion or mixing with several pure CO₂ sources that have
360 more than a single composition for $\delta^{13}\text{C}$.

361 The value [obtained from equation \(3\)](#) reflects a general trend in the range of the isotopic
362 variations of the different possible sources. [Therefore](#), the $\delta^{13}\text{C}$ of the 'pure-CO₂' end-member
363 is always an apparent value, which must be interpreted with the help of additional hypotheses
364 or additional information, or both.

365 If data point (air mixtures) all lie close to a best-fit line, the conclusion is often drawn that all
366 the points represent mixtures between atmospheric air and a single pure-CO₂ end-member. In
367 practice, data often scatters closely around a best-fit line and it can be attributed either to
368 measurement and sampling errors or to composition fluctuations of the pure-CO₂ end-
369 member. When the scatter is greater, other models have to be considered (e.g., diffusion or
370 mixing with other CO₂ sources).

371 In this work, the conceptual frame [established](#) for the fieldwork and data analysis is essentially
372 based on advective and diffusive CO₂ exchange between exterior atmosphere, soil and the
373 caves environments (according to Fig. 1). On the basis of previous work carried out in these
374 sites (Fernandez-Cortes et al., 2009; Garcia-Anton, 2014b; Fernandez-Cortes et al., 2015; Pla et
375 al., 2016), we assume that drip water CO₂ degassing is present but its contribution to the total
376 CO₂ concentration of the underground environments is considered negligible compared to the
377 transport processes in gaseous phase (i.e. advection or diffusion).

378 The applicability of the Keeling plot has been proven in environments where the mixing
379 process between air masses occurs by bulk advection (Bowling and Massman, 2011; Buchmann
380 et al., 1998; Zobitz et al., 2006). However, the assumption of the model for diffusive
381 environments (e.g., from the air-filled porosity of soils to the open atmosphere) could lead to
382 misinterpretation relative to the isotopic [ratio](#) of the source (Risk and Kellman, 2008;
383 Nickerson and Risk, 2009). The diffusive process introduces an isotopic fractionation in the CO₂

384 input to the resulting concentration (established at -4.4‰ in stationary conditions, Craig, 1953;
385 Cerling et al., 1991). Then, the value obtained with the model refers to the isotopic ratio of the
386 CO₂ that enhances the concentration, which is different from the original due to the
387 fractionation suffered during the mixing process.

388 **3 Results**

389 3.1 Exterior samples

390 The CO₂ recorded in the exterior atmosphere of the studied field sites varied over a narrow
391 range both among sites (399.1 to 476.4 ppm; Table 2, 3) as well as temporally within sites (less
392 than 32 ppm). The δ¹³C of CO₂ showed a modest range among sites (-13.2 to -8.2‰) but minor
393 temporal variations (less than 2.6‰). These values are consistent to clean atmospheric
394 conditions slightly modified by organic activity due to the proximity of the sampling to the
395 surface. In each field campaign, the variability in the parameters was relatively low, with
396 maximum ranges of variation of 97.5 ppm and 3.6‰ for CO₂ and δ¹³CO₂, respectively.

397 3.2 Soil samples

398 Soil-contained CO₂ mean values ranged from 935.5 to 8116.1 ppm and the δ¹³CO₂ from -27.2
399 to -18.8‰ (Fig. 8, Table 2). The soil CO₂ concentration was always greater and its isotopic ratio
400 was always lighter than those of the exterior air. In general terms, soil samples presented
401 much greater range both spatially as well as temporally in the soil CO₂ (compared to
402 atmosphere). Castañar de Ibor cave presented the maximum soil CO₂ concentration (9461.2
403 ppm in November 2011) and the greatest seasonal range (8974.9 ppm, Table 3). Highest soil
404 δ¹³CO₂ was observed in Rull cave (-15.3‰ in July 2014), which also presented the greatest
405 seasonal range (10.2‰, Table 3). Lower soil concentrations of CO₂ correspond to higher values
406 of δ¹³CO₂, which in general, were observed in summer months (Fig. 8, Table 2). This set of

407 values is in concordance with mixed atmospheric air and soil-produced CO₂ with a $\delta^{13}\text{C}_{\text{CO}_2}$
408 around -27‰ (for C3-type land plants, Amundson et al., 1998).

409 3.3 Cave samples

410 All of the samples obtained presented higher concentrations of CO₂ and lower $\delta^{13}\text{C}_{\text{CO}_2}$ than
411 those of the exterior air. Mean values of CO₂ concentration and $\delta^{13}\text{C}_{\text{CO}_2}$ for each field campaign
412 were from 457.7 ppm to 5678 ppm and from -26.4‰ to -12.1‰ (Fig. 8, Table 2). Altamira cave
413 presented the highest absolute CO₂ concentration (6214.7 ppm in November 2011) and the
414 greatest seasonal range (5886.8 ppm, Table 3). Lowest absolute CO₂ concentration was
415 observed in Ojo Guareña cave (415.02 ppm in June 2014) and the lowest annual range was
416 observed in Rull cave (2330.4 ppm). Minimum $\delta^{13}\text{C}_{\text{CO}_2}$ was registered in Altamira cave (-26.7‰
417 in March 2015) and the lowest annual range was observed in Castañar de Ibor cave (4.3‰).
418 Maximum $\delta^{13}\text{C}_{\text{CO}_2}$ was registered in Ojo Guareña cave (-8.2‰ in June 2014), which also
419 presented the greatest seasonal range (10.2‰, Table 3). Altamira and Castañar de Ibor caves
420 presented their minimum CO₂ concentration and maximum $\delta^{13}\text{C}_{\text{CO}_2}$ in the summer season
421 while their winter months are characterized by higher CO₂ values and minimum $\delta^{13}\text{C}_{\text{CO}_2}$. The
422 opposite pattern was observed in Ojo Guareña, Rull and El Sidron caves (Fig.8, Table 2).

423 3.4 Estimation of the $\delta^{13}\text{C}$ of the CO₂ source

424 Isotope and CO₂ concentration values have been used to estimate the isotopic **ratio** of the CO₂
425 source ($\delta^{13}\text{C}_s$) using the Keeling plot method (Fig. 9). The intercept values of the Keeling plot
426 ($\delta^{13}\text{C}_s$) for the samples collected over a year at each field site were -27.7‰ (Altamira), -25.9‰
427 (Castañar), -26.7‰ (Ojo Guareña), -27.6‰ (Rull) and -27.5‰ (El Sidron). These values indicate
428 a prevalence of C3 plant activity in these systems (around -27‰, Amundson et al., 1998).

429 Two Keeling plots were obtained for each sampling field campaign (Table 2, Fig. 10) taking into
430 account: 1) all samples collected (in the exterior, in the soil above the cave and inside the cave)

431 and 2) the samples collected in the exterior air and in the soil. As a result, the temporal
432 variations in 1) the isotopic **ratio** of the source for the entire system ($\delta^{13}\text{C}_s\text{-system}$) and 2) the
433 isotopic **ratio** of the soil-produced CO_2 ($\delta^{13}\text{C}_s\text{-soil}$) were obtained. The $1/\text{CO}_2$ and $\delta^{13}\text{CO}_2$ values
434 fit the Keeling model with a coefficient of determination that was higher than 0.9 ($R^2 > 0.9$).
435 $\delta^{13}\text{C}_s\text{-system}$ ranged from -24.7‰ and -29.8‰ and $\delta^{13}\text{C}_s\text{-soil}$ ranged from -21.5‰ to -29.4‰
436 (Table 2).

437 The values obtained at each field site exhibited seasonal patterns. Lower values of the isotopic
438 **ratios** of the sources ($\delta^{13}\text{C}_s\text{-system}$, $\delta^{13}\text{C}_s\text{-soil}$) were observed during the wetter and colder
439 months, while a trend to heavier values was observed in the dryer and warmer months.
440 Differences between the $\delta^{13}\text{C}_s\text{-system}$ and $\delta^{13}\text{C}_s\text{-soil}$ in the studied caves alternated their
441 relative roles of heavier/lighter with a common trend towards $\delta^{13}\text{C}_s\text{-system} < \delta^{13}\text{C}_s\text{-soil}$ during
442 drier and warmer climatic conditions (Fig. 8).

443 **4 Discussion**

444 4.1 Temperature versus soil moisture control on CO_2 and $\delta^{13}\text{CO}_2$ in soil air

445 The CO_2 concentration and the $\delta^{13}\text{CO}_2$ of the air contained in the soil at each field site varied
446 throughout the year (Fig. 8). It is well known that variations in soil CO_2 concentration and
447 therefore in $\delta^{13}\text{CO}_2$ are regulated by both biotic and abiotic processes (Moyes et al., 2010;
448 Kayler et al., 2010). The organic respiration in soil by heterotrophic and autotrophic organisms
449 is mainly determined by soil temperature and moisture. Moreover, gas transfer processes
450 between soil and the exterior air, which determines the soil efflux, play an important role in
451 the soil CO_2 concentration. The increase in CO_2 production with the increase in temperature
452 has been well demonstrated in a wide number of studies (Lloyd and Taylor, 1994; Fang and
453 Moncrief, 2001; Risk et al., 2002). However, the cause-effect relationship between soil
454 moisture and soil CO_2 efflux is not well defined (Fang and Moncrief, 2001; Vicca et al., 2014).
455 Soil CO_2 productivity is directly dependent on soil moisture with a relationship particularly

456 marked along the annual cycle by significant responses to rain events (Xu et al., 2004).

457 Moreover, extremely wet soil conditions decrease the gas diffusivity in the soil (Hashimoto and
458 Komatsu, 2006; Jabro et al., 2012), which could favour an increase on the soil CO₂
459 concentration. The Altamira and Castañar caves have a continuous record of the volumetric
460 water content (VWC) during the sampling periods analysed here. The δ¹³CO₂ of the samples
461 collected at the Altamira and Castañar field sites shows a well-defined linear relationship with
462 the soil moisture, expressed as the volumetric water content (VWC, (Fig. 8 and Fig. 11B)).

463 Throughout the studied cycles, the lower δ¹³CO₂ corresponded to higher CO₂ concentrations in
464 the soil, marking the lower influence of exterior air in the CO₂ contained in the soil (Fig. 11B).

465 This relationship seems to be essentially driven by soil moisture. The increase in soil water
466 content increases respiration rates and decreases diffusivity, which increases belowground CO₂
467 with an isotopic ratio that is closer to the characteristic value of organic CO₂ production
468 (lighter values). This relationship is characteristic for each field-site, pointing to a dependence
469 on the specific vegetation, soil properties (organic matter, microbiological activity, etc.) and
470 physical and/or climatic features. Although soil moisture has not been monitored in Ojo
471 Guareña, Rull and El Sidron caves, these observations are also consistent with the data
472 collected in these sites (Fig. 8). Soil CO₂ and δ¹³CO₂ seasonal variations can be observed linked
473 to the annual climate cycle in which high soil CO₂ and light δ¹³CO₂ values are characteristic of
474 wetter and colder months.

475 Regarding the temperature control on soil CO₂ and δ¹³CO₂, heavier values are observed during
476 the summer stages in all the studied sites (Fig. 8). This probably reflects higher rates of soil-
477 atmosphere exchange as a consequence of lower water content in the soils.

478 According to the observations, connection between soil and exterior air masses and
479 respiration rates control soil CO₂ (g) concentration and its δ¹³C. High humidity conditions
480 during the rainy season favour production and storage of CO₂ in the soil's pore space.

481 4.2 Sources of variation in $\delta^{13}\text{C}$ of soil-produced CO_2

482 The isotopic **ratio** of the source to the soil ($\delta^{13}\text{C}_s\text{-soil}$) distinguishes the variations in the
483 isotopic **ratio** of the soil-produced CO_2 , irrespective of the influence of exterior air, according
484 to the assumed two-end member model (i.e., the air contained in the soil is a mixture of
485 exterior air and soil-produced CO_2). The obtained isotopic **ratio** of the source in the soil ($\delta^{13}\text{C}_s\text{-}$
486 soil) for each field campaign carried out in the Altamira and Castañar de Ibor caves (Table 2)
487 was compared with the mean values of soil moisture recorded during each field campaign (Fig.
488 8 and 12). The set of data pairs have a common logarithmic downward trend pointing to
489 common processes driving the isotopic **ratio** of the source of CO_2 in the soil. Heavier values for
490 the isotopic ratio of the source in the soil are characteristic of drier conditions, whereas lighter
491 values correspond to higher soil moisture (Fig. 12).

492 The results reported here are consistent with many previous studies, in which a heavier
493 isotopic source value is observed during drier and warmer seasons compared to the colder and
494 wetter months of the year (Ekberg et al., 2007; Marron et al., 2009; Goffin et al., 2014). Other
495 studies have related the variations in the $\delta^{13}\text{C}$ of ecosystem and soil respiration to air humidity
496 (Ekblad and Högberg, 2001; Bowling et al., 2002; Ekblad et al., 2005). This parameter is used as
497 an index of plant moisture stress known to influence the isotopic discrimination during
498 photosynthesis (Farquhar et al., 1982). This effect is observed in environments with a strong
499 seasonality in the moisture contained in the air. However, the characteristic humid climate of
500 the Altamira field site (Table 1, Fig. 8) maintains a monthly average relative humidity above
501 70% during the entire year, with values above 90% most of the year (Sanchez-Moral et al.,
502 1999; Cuezva et al., 2009). Thus, seasonal variations observed in $\delta^{13}\text{CO}_2$ of soil respiration at
503 Altamira contrast the explanation based on moisture stress suffered by the autotrophic
504 organisms in drier conditions.

505 Advection and diffusion mechanisms are responsible for soil CO₂ transport to the atmosphere
506 and to the underground system. While advection supposes a bulk movement of air without
507 modification of the isotopic ratio of the source for the displaced air mas (soil air into the
508 exterior), diffusion affects the isotopic ratio of the displaced gas during the process (Nickerson
509 and Risk, 2009). Due to the weight difference between ¹³C and the major isotopologue of C,
510 ¹²C, the diffusive movement of the gas results into an enlightenment of the displaced gas
511 regarding to its original isotopic ratio. As a result, the CO₂ of the pool source (in this case the
512 soil) could result heavier than the produced CO₂ if diffusive transport of the gas is considerably
513 greater than production. The isotopic fractionation by diffusion is theoretically estimated in -
514 4.4‰ (Cerling et al., 1984) but it is known that this ratio could be rather variable (Davidson,
515 1995). According to this, an increase of diffusion in soil would lead to heavier δ¹³CO₂ values.
516 This effect could be occurring in our study sites as we have observed heavier values of the CO₂
517 source in the soil during drier periods in which less soil humidity would induce an increase of
518 the gas diffusivity (Jabro et al., 2012).

519 Figure 13A presents the measurements on soil gas at the 5 fieldworks sites as a Keeling plot,
520 including the functions modelling either the diffusion from a gas source and the advection and
521 mixing with atmospheric air. The grey-shaded area in Figure 13A includes the soil air affected
522 by the mixing between background atmosphere and the apparent composition of pure CO₂
523 produced by microbial respiration in soil. To model the mixing of pure CO₂ with atmospheric
524 air, a theoretical concentration of CO₂ of 20000 ppm (twice the maximum concentration
525 measured in the soil samples, roughly 9500 ppm) and a δ¹³C ranging -26 to -28‰ for pure CO₂
526 produced by microbial respiration in soils containing organic matter from C3 vegetation
527 (according to Amundson et al., 1998) were considered. The black-solid straight lines of the
528 mixing area are labeled as % of pure additional CO₂ remaining in the soil air.

529 Air contained in soil above Altamira cave (particularly during summer months) is well mixed
530 with background atmosphere and the pure CO₂ remaining in soil samples are usually below
531 10%. By contrast, in poor-ventilated soils the pure CO₂ remaining is higher than 10%. The wide
532 scatter of data in soil air from Ojo Guareña, Rull and Castañar is attributed to two processes
533 acting in combination: 1) mixing of pure CO₂ with atmospheric air and 2) isotopic fractionation
534 of carbon in CO₂ as the gas diffuses from the soil pore-space into some other reservoir (e.g.
535 epikarst or open atmosphere). The curved arrows in Figure 13A show the kinetic fractionation
536 trajectory of soil CO₂ due to its upwards diffusion to open atmosphere or epikarst, modelled by
537 a Rayleigh-type distillation process with a fractionation coefficient of 4.4‰ (based on the
538 theoretical mass-dependent fractionation between ¹²CO₂ and ¹³CO₂ during diffusion, according
539 to Camarda et al., 2007). The Rayleigh equation is an exponential relation that describes the
540 partitioning of isotopes between two reservoirs as one-reservoir decreases in size, in this case
541 the CO₂ content in soil air. Each curve arrow starts from a soil air with a different percentage of
542 remaining pure CO₂ produced by respiration in soil. The black-solid curve starts from a
543 theoretical source of CO₂ (2% CO₂ and -27‰ δ¹³CO₂) and the dashed arrows from a certain
544 percentage of pure additional CO₂ (20% and 50% remaining, respectively). As an example, the
545 curve arrow that starts from a 20% remaining of pure CO₂ has been labelled with the fraction
546 of CO₂ remaining after Rayleigh fractionation associated to the diffusion process. In areas with
547 lower annual rainfall rates such as Ojo Guareña, Castañar and Rull (Table 1), most of the soil air
548 samples fit well to these diffusion curves and, therefore, this indicates an effective diffusion of
549 CO₂ from soil to open atmosphere or to deeper soils locations and epikarst zone. Soil air with a
550 remaining pure CO₂ that ranges between 50% and 20% undergoes gas diffusion and the
551 resulting air mixtures measured in soil usually have a remaining fraction of soil-derived CO₂
552 between 0.2 and 0.5.

553 According to the above discussion, the diffusive transport of the gas is likely responsible for the
554 temporal variations observed in the isotopic [ratio](#) of the soil-produced CO₂ in the sites studied

555 here (Fig. 8). Reduction of soil humidity during the drier season, due to less rainfall and
556 increase of temperatures, promotes diffusion of soil produced CO₂ to the atmosphere, deeper
557 soil layers or the epikarst. This effect would produce an enrichment of the soil contained CO₂,
558 which in last term causes an overestimation of the CO₂ source isotopic ratio ¹³C/¹²C (organic
559 production). Diffusion of the gas during dry season must play a major role on the gas transport
560 process to the atmosphere, as it is strong enough to modify the isotopic signal of organic
561 produced CO₂.

562 Some cave end-members of Keeling plots have a higher δ¹³C than their corresponded soil-
563 produced gas, which indicate that, in these cases, there are more processes involved on CO₂-
564 transport beside the diffusion. Consequently, the added CO₂ does not directly come from the
565 soil. The Keeling plots for soil air show considerable non-linear scatter in some cases (Fig. 13A)
566 and this indicates that the soil data do not correspond exactly to δ¹³C of the CO₂ fluxes
567 produced in the soil. CO₂ data measured in soil air is actually derived from the local diffusion in
568 the soil. This results in a preferential loss of the light isotopic fraction with remaining CO₂
569 which becomes isotopically heavier (higher δ¹³C) than the CO₂ actually produced in the soil.

570 4.3 Ventilation versus soil CO₂ production regulating CO₂ and δ¹³CO₂ in the caves

571 Each cavity has a characteristic environmental variability over an annual cycle (Fig. 8). It is
572 known that the level of ventilation is determined by geomorphology, is regulated by weather
573 variations and is therefore different in every cave (Bourges et al., 2001). In Altamira, Castañar
574 de Ibor, Ojo Guareña and Rull caves, correlation between radon-222 (²²²Rn) and CO₂ monthly
575 average values showed lineal trends marking a common influence of the ventilation of the
576 underground environments on both gases (Fig. 14). Active ventilation shifts the cave
577 environments towards conditions that are more similar to that of the exterior atmosphere
578 (lower concentration of CO₂ and ²²²Rn, and higher values of δ¹³CO₂, Fig. 9 and Fig. 14), whereas
579 the isolation of the caves favours an increase in CO₂ and ²²²Rn, and a decrease in δ¹³CO₂.

580 Lower correlation of the ^{222}Rn - CO_2 values was observed in Castañar de Ibor compared to the
581 other sites pointing to an important influence of other-than-ventilation processes on the cave
582 air CO_2 . This cave is poorly ventilated compared to the other caves and presents a CO_2
583 concentration always above 2000 ppm (Table 2, Fig.8). Cave air ^{222}Rn concentration (>20000
584 Bq/m^3) is also much greater than the other cavities due to the high content on uranium of the
585 rock in this site (Alvarez-Gallego et al., 2015). Differences between the parameters could be
586 due to the distinct recharge velocities. While radon exhalation is produced at a constant rate
587 characteristic of each rock (Cigna, 2005), CO_2 inlet to the cave is linked to variations on the CO_2
588 concentration of the soil and the vadose zone, which may vary throughout the year. If
589 ventilation does not exclusively control gases concentration inside Castañar de Ibor cave,
590 differences between the gases recharge velocities could be related to different factors
591 controlling gases production. In the case of Castañar cave, the scatter in some of the Rn - CO_2
592 correlations suggests that Rn is produced at a different location from CO_2 . According to the
593 findings from our previous studies, the weathering leakage process of the bedrock favours the
594 remobilization of radionuclides (i.e. radon source) via leaching and their later settlement into
595 the cave environment associated to mineral phases of cave deposits (Garcia-Guinea et al.,
596 2013).

597 According to previous results, the Altamira and Castañar caves undergo an isolation period
598 during the cold and wet season and a preferential ventilation period during summer (Fig. 8,
599 Cuezva et al., 2009; Fernandez-Cortes et al., 2011). The Ojo Guareña and Rull caves agree with
600 preliminary studies (Fernandez-Cortes et al., 2015a; Pla et al., 2015) in which the period of
601 major ventilation is produced during the colder months of the year (Fig. 8). The results of the
602 samplings carried out inside El Sidron cave indicate that the colder season is the period of
603 major connection with the exterior atmosphere (Table 2).

604 The goodness of fit of the Keeling plots (Fig. 9) obtained with all of the samples collected in
605 each cavity points to the CO₂ derived from roots respiration and soil organic matter (SOM)
606 degradation as the main source of CO₂. Though SOM degradation could occur in the vadose
607 zone (Noronha et al., 2015; Matthey et al., 2016), the caves here studied are quite shallow
608 (except Ojo Guareña, Table 1), which reduces probability of SOM accumulation in the epikarst.

609 The distribution of the points in the Keeling plots highlights the characteristics and variability
610 (referring to CO₂ and δ¹³CO₂) of each underground environment during the studied intervals
611 (Fig. 9). The cave samples collected at Altamira, Castañar de Ibor and Rull were more similar to
612 the soil samples, supporting the prevalence of the soil-produced CO₂ inlet into the caves. The
613 Ojo Guareña and El Sidron caves had more scattered distributions of the points with a general
614 trend to values closer to the exterior air conditions, indicating an important influence of the
615 active ventilation during the majority of the year.

616 Figure 13B shows that cave air compositions result from mixing between atmospheric air and a
617 CO₂-rich component with lighter isotopic compositions that lies in the range -26 to -28 ‰.
618 These δ¹³CO₂ values are substantially lighter in comparison with those obtained in Gibraltar
619 caves, which lie in the range -18 to -24‰ (Matthey et al., 2016). This difference of δ¹³CO₂ values
620 indicates that CO₂ source is not related to ground air that comes from the decay of organic
621 material washed down into the deep soil and unsaturated zone.

622 The black-solid straight line of the mixing area is labeled as % of pure additional CO₂ from soil
623 remaining in the cave air (perpendicular dotted lines). The modelling of pure CO₂ mixing with
624 atmospheric air considers both the averaged composition of the background atmosphere of
625 the studied sites and a theoretical (and apparent) source of pure CO₂ (2% CO₂ and δ¹³CO₂
626 ranging -26 to -28 ‰). Cave air is well mixed with background atmosphere in highly ventilated
627 sites as Ojo Guareña and Sidron, so that the remaining soil-derived CO₂ is usually below 3%,
628 with a marked seasonal variation. By contrast, in poor-ventilated caves as Castañar or, even,

629 Altamira cave during some periods when air renewal is hindered, the remaining soil-derived
630 CO₂ is usually above 5%.

631 4.4 δ¹³C of the source of CO₂ in the soil-underground system

632 The high correlation of the [1/CO₂, δ¹³CO₂] data pairs obtained for the samples collected in the
633 soil, the caves and the exterior air (Fig. 9) indicates that the soil and the underground
634 environment form a system with good communication. Similar high correlations have been
635 described in other studies (Breecker et al., 2012). The soil-produced CO₂ displaces towards the
636 underground air filled spaces, including voids, cracks and cavities. Therefore, the values
637 obtained for the isotopic ratio of the system (δ¹³C_{s-system}) characterize the zone immediately
638 below the surface, including soil, host rock and cave and, therefore, it indicates the likely
639 average values of δ¹³C of CO₂ in ground air at each site. This value would then characterize the
640 air under the surface, which can be released to the exterior atmosphere as a result of
641 ventilation affecting soil and epikarst.

642 Recent studies have demonstrated an important source of CO₂ in caves located in the air-filled
643 pore space between soil and cave (called “ground air”). Within pore space, organic decay
644 processes would increase the isotopic signal of soil-produced CO₂. We have tested this
645 hypothesis by comparing our data with those obtained for St. Michaels cave (Mattey et al.,
646 2016, Figure 13B). The isotopic ratios of the samples collected in St. Michaels are heavier than
647 the isotopic ratios observed in our caves. This could be due to a less influence of the ground
648 reservoir in our study sites, as our locations are significant less deeper (St. Michaels cave is
649 located at >100m depth, Mattey et al. 2016). Moreover, the proximity of St. Michaels cave to
650 the sea enhances the rate of water-rock interaction and would lead to more positive values of
651 δ¹³C of cave air.

652 The set of values obtained for δ¹³C_{s-system} at Altamira and Castañar de Ibor for each field
653 campaign exhibited a downward logarithmic trend with soil moisture (Fig. 15). The isotopic

654 ratio of the source in the system had heavier values as the soil moisture decreased. The
655 correlation of the set of points to the obtained function is, in this case, higher than that
656 obtained with the set of values for $\delta^{13}\text{C}_s$ -soil. Consequently, there could be a common control
657 over the isotopic ratio of the source of the CO_2 contained in the soil and the CO_2 contained in
658 the underground system. According to this, the increase of diffusion related to the reduction
659 of soil humidity would shift the isotopic ratio of the source in the soil towards higher values
660 due to fractionation effect during the transport process to the atmosphere. As a result, the CO_2
661 reservoir located in the soil would have an isotopic signal heavier during the drier season than
662 during the rainy months of the year. Therefore, the CO_2 source for the underground system
663 would be also affected by the seasonal enrichment of the isotopic ratio.

664 According to the trend obtained as a function of the soil volumetric water content in the two
665 emplacements analysed, the isotopic ratio of the source in the systems ranged between -
666 20.29‰ and -28.16‰ for the boundary conditions of soil moisture (Fig. 15). The boundary
667 conditions have been taken as the accuracy of the VWC probe (0.01%) and the maximum of
668 the soil porosities between the specific monitored sites (i.e. 48% in Altamira field site). Under
669 lowest levels of soil volumetric water content, the underground contributes an isotopic ratio of
670 around -20.29‰, representing the isotopic ratio of the CO_2 stored in the underground system.
671 When soil is completely water saturated, the CO_2 stored underground is more similar than
672 organically produced CO_2 with values around -28.16‰. The CO_2 with a characteristic light $\delta^{13}\text{C}$
673 stored under the surface -in the air filling space contained in the soil and the rock (including
674 the cave)- could be released to the exterior atmosphere as a result of ventilation.

675 Alternatively, the range of temporal variations of $\delta^{13}\text{C}_s$ -system was lower compared to that of
676 $\delta^{13}\text{C}_s$ -soil for the Altamira, Castañar de Ibor, Ojo Guareña and Rull caves (Fig.8). There appears
677 to be a damping effect over the isotopic ratio of the soil-produced CO_2 descending towards the
678 caves. This points to a slow transference of the gas from soil to the underground, buffering the

679 rapid variations in the isotopic ratio throughout deeper zones. However, the absence of a lag
680 between the $\delta^{13}\text{C}_s$ -system and the $\delta^{13}\text{C}_s$ -soil signals could also imply that CO_2 is transported
681 into the cave by advective mechanism.

682 The temporal evolution of the $\delta^{13}\text{CO}_2$ of the source presents seasonal variations due to the
683 processes affecting the system driven by variations in weather. There was a general trend at
684 the different field sites towards lower values of the $\delta^{13}\text{CO}_2$ of the source during wetter and
685 colder conditions. On the contrary, heavier values were obtained in drier and warmer
686 conditions (Fig. 8). In the sites studied here, the isotopic ratio of the source in the system
687 ($\delta^{13}\text{C}_s$ -system) was between 1 and 3‰ heavier during the summer than during the winter (Fig.
688 2 and Table 2). Moreover, the greatest differences between $\delta^{13}\text{C}_s$ -soil and $\delta^{13}\text{C}_s$ -system are
689 observed in caves located in the zone of Mediterranean climate with higher mean temperature
690 and lower annual precipitation rate (Castañar de Ibor, and Rull caves, Table 1). According to
691 the results, the gas transport processes occurring and affecting the isotopic ratio of the soil-
692 produced CO_2 seem to drive the seasonal evolution of the isotopic ratio characteristic of the
693 CO_2 stored in the underground system ($\delta^{13}\text{C}_s$ -system, Fig. 2).

694 **5 Conclusions**

695 The present study has shown that joint characterization of CO_2 concentration and $\delta^{13}\text{CO}_2$ from
696 cave and soil air and exterior atmosphere is a useful and suitable method for characterizing the
697 sources and processes involved in the CO_2 exchanges between shallow underground systems
698 and the troposphere on an annual scale. The values obtained in the monthly and bimonthly
699 field campaigns in several distinct caves identified seasonal patterns in the isotopic ratio of soil
700 air and the underground atmosphere. The $\delta^{13}\text{CO}_2$ marks periods of isolation/ventilation,
701 whereby the caves alternate their role as a reservoir or source of CO_2 on an annual scale.
702 These data are consistent with the annual microclimatic behaviour characteristics for each

703 cavity and their respective locations. All of the cases confirmed that the CO₂ contained in the
704 cave is originated as the result of the organic activity supported in the overlying soil.

705 Climate models predict an intensification of extreme events (Ciais et al., 2013). Previous
706 studies have demonstrated that among them, drought has the strongest impact on terrestrial
707 carbon cycling (Frank et al., 2015). Specifically, droughts have observed to produce a
708 substantial reduction of the ecosystems carbon sink capability (Ciais et al., 2005, Schwalm et
709 al., 2012), which results on positive carbon-climate feedbacks. This study shows an increase of
710 CO₂ emissions from subsoil linked to dry periods in 5 different locations with 2 distinct
711 climates. Therefore, the CO₂ release from vadose zone may contribute to the atmospheric CO₂
712 enhancement resulted from the intensive droughts expected throughout the present century
713 because of climate change.

714 **Acknowledgements**

715 This research was funded by the Spanish Ministry of Economy and Competitiveness projects
716 CGL2016-78318-C2-1R and CGL2016-78318-C2-2R [AEI/FEDER/UE](#) and its programme Torres
717 Quevedo (PTQ 13-06296). Funding was also provided by the People Programme (Marie Curie
718 Actions-Intra-European Fellowships, call 2013) of the European Union's Seventh Framework
719 Programme (FP7/2007-2013) under the REA grant agreement nº 624204. We thank the cave
720 managers for their collaboration throughout the entire investigation.

721 **References**

722 AEMET-IM, 2011. Iberian Climate Atlas. Air temperature and precipitation (1971-2000) in
723 Agencia Estatal de Metereologia (España), Instituto de Metereologia (Portugal) (Eds.)
724 <http://www.aemet.es/es/conocerlas/publicaciones/detalles/Atlas-climatologico>

725 Alonso-Zarza, A.M., Martin-Perez, A., Martin-Garcia, R., Gil-Pena, I., Melendez, A., Martinez-
726 Flores, E., Hellstrom, J., Munoz-Barco, P., 2011. Structural and host rock controls on the

727 distribution, morphology and mineralogy of speleothems in the Castanar Cave (Spain). *Geol.*
728 *Mag.* 148, 211-225.

729 Alvarez-Gallego, M., Garcia-Anton, E., Fernandez-Cortes, A., Cuezva, S., Sanchez-Moral, S.,
730 2015. High radon levels in subterranean environments: monitoring and technical criteria to
731 ensure human safety (case of Castañar cave, Spain). *J. Environ. Radioactiv.* 145, 19-29.

732 Amundson, R., Stern, L., Baisden, T., Wang, Y., 1998. The isotopic composition of soil and soil-
733 respired CO₂. *Geoderma* 82, 83-114.

734 Baldini, J.U.L., Baldini, L.M., McDermott, F., Clipson, N., 2006. Carbon dioxide sources, sinks,
735 and spatial variability in shallow temperate zone caves: Evidence from Ballynamintra Cave,
736 Ireland. *J. Cave Karst Stud.* 68, 4-11.

737 Berner, R.A., 2003. The long-term carbon cycle, fossil fuels and atmospheric composition.
738 *Nature* 426, 323-326.

739 Bourges, F., Mangin, A., d'Hulst, D., 2001. Le gaz carbonique dans la dynamique de
740 l'atmosphère des cavités karstiques : l'exemple de l'Aven d'Orgnac (Ardèche). *C.R. Acad. Sci.,*
741 *Ser. Ila: Earth Planet. Sci.* 333, 685-692.

742 Bowling, D., McDowell, N., Bond, B., Law, B., Ehleringer, J., 2002. 13C content of ecosystem
743 respiration is linked to precipitation and vapor pressure deficit. *Oecologia* 131, 113-124.

744 Bowling, D.R., Massman, W.J., 2011. Persistent wind-induced enhancement of diffusive CO₂
745 transport in a mountain forest snowpack. *J. Geophys. Res. Biogeo.* 116, G04006.

746 Bowling, D.R., Ballantyne, A.P., Miller, J.B., Burns, S.P., Conway, T.J., Menzer, O., Stephens,
747 B.B., Vaughn, B.H., 2014. Ecological processes dominate the 13C land disequilibrium in a Rocky
748 Mountain subalpine forest. *Global Biogeochem. Cy.* 28, 352–370.

749 Breecker, D.O., Payne, A.E., Quade, J., Banner, J.L., Ball, C.E., Meyer, K.W., Cowan, B.D., 2012.
750 The sources and sinks of CO₂ in caves under mixed woodland and grassland vegetation.
751 *Geochim. Cosmochim. Acta* 96, 230-246.

752 Buchmann, N., Hinckley, T.M., Ehleringer, J.R., 1998. Carbon isotope dynamics in *Abies*
753 *amabilis* stands in the Cascades. *Can. J. Forest Res.* 28, 808-819.

754 Camacho, A.I., Valdecasas, A.G., Rodriguez, J., Cuezva, S., Lario, J., Sanchez-Moral, S., 2006.
755 Habitat constraints in epikarstic waters of an Iberian Peninsula cave system. *Ann. Limnol. Int. J.*
756 *Lim.* 42, 127-140.

757 Camarda, M., Gregorio, S.D., Favara, R., Gurrieri S., 2007. Evaluation of carbon isotope
758 fractionation of soil CO₂ under an advective-diffusive regimen: a tool for computing the
759 isotopic composition of unfractionated deep source. *Geochim. Cosmochim. Acta* 71, 3016–
760 3027.

761 Cerling, T.E., 1984. The stable isotopic composition of modern soil carbonate and its
762 relationship to climate. *Earth Pl. Sc. Lett.* 71, 229-240.

763 Cerling, T.E., Solomon, D.K., Quade, J., Bowman, J.R., 1991. On the isotopic composition of
764 carbon in soil carbon-dioxide. *Geochim. Cosmochim. Acta* 55, 3403-3405.

765 Chen, X., Wang, W., Luo, G., Ye, H., 2014. Can soil respiration estimate neglect the contribution
766 of abiotic exchange? *J. Arid Land* 6, 129-135.

767 Christoforou, C.S., Salmon, L.G., Cass, G.R., 1996. Air exchange within the Buddhist cave
768 temples at Yungang, China. *Atmos. Environ.* 30, 3995-4006.

769 Choppy, J., 1983. Phénomènes Karstiques: Dynamique de l'air. *Processus Climatiques . Spéléo*
770 *Club de Paris et Club Alpin Français.* Paris, 84 pp.

771 Ciais, P., Sabine, C., Bala, G., Bopp, L., Brovkin, V., Canadell, J., Chhabra, A., DeFries, R.,
772 Galloway, J., Heimann, M., Jones, C., Le Quéré, C., Myneni, RB., Piao, S., Thornton, T., 2013.
773 Carbon and Other Biogeochemical Cycles. In: Stocker, T.F., Qin, D., Plattner G.K., Tignor, M.,
774 Allen S.K., Boschung J., Nauels A., Xia Y., Bex, V., Midgley, P.M. (Eds). Climate change 2013: The
775 Physical Science Basis (chapter 6), Contribution of Working Group I to the Fifth Assessment
776 Report of the Intergovernmental Panel on Climate Change. Cambridge Univ. Press, Cambridge,
777 pp. 465-570.

778 Ciais, P., Reichstein, M., Viovy, N., Granier, A., Ogee, J., Allard, V., Aubinet, M., Buchmann, N.,
779 Bernhofer, C., Carrara, A., Chevallier, F., De Noblet, N., Friend, A.D., Friedlingstein, P.,
780 Grunwald, T., Heinesch, B., Keronen, P., Knohl, A., Krinner, G., Loustau, D., Manca, G.,
781 Matteucci, G., Miglietta, F., Ourcival, J.M., Papale, D., Pilegaard, K., Rambal, S., Seufert, G.,
782 Soussana, J.F., Sanz, M.J., Schulze, E.D., Vesala, T., Valentini, R., 2005. Europe-wide reduction in
783 primary productivity caused by the heat and drought in 2003. Nature 437, 529-533.

784 Cigna, A.A., 2005. Radon in caves. Int. J. Speleol. 34, 1-18.

785 Craig, H., 1953. The geochemistry of the stable carbon isotopes. Geochim. Cosmochim. Acta 3,
786 53-92.

787 Crosson, E.R., 2008. A cavity ring-down analyzer for measuring atmospheric levels of methane,
788 carbon dioxide, and water vapor. Appl. Phys. B-Lasers O. 92, 403-408.

789 [Cuezva, S., 2008. Dinámica microambiental de un medio kárstico somero \(Cueva de Altamira,](#)
790 [Cantabria\): microclima, geomicrobiología y mecanismos de interacción cavidad-exterior. Ph. D.](#)
791 [Thesis, Universidad Complutense de Madrid, Madrid, p. 320.](#)

792 Cuezva, S., Sanchez-Moral, S., Saiz-Jimenez, C. and Cañaveras J.C., 2009. Microbial
793 Communities and Associated Mineral Fabrics in Altamira Cave, Spain. Int. J. Speleol. 38 83-92.

794 Cuezva, S., Fernandez-Cortes, A., Benavente, D., Serrano-Ortiz, R., Kowalski, A.S., Sanchez-
795 Moral, S., 2011. Short-term CO₂(g) exchange between a shallow karstic cavity and the external
796 atmosphere during summer: Role of the surface soil layer. *Atmos. Environ.* 45, 1418-1427.

797 Davidson, G.R., 1995. The stable isotopic composition and measurement of carbon in soil CO₂.
798 *Geochim. Cosmochim. Acta* 59, 2485-2489.

799 Ekberg, A., Buchmann, N., Gleixner, G., 2007. Rhizospheric influence on soil respiration and
800 decomposition in a temperate Norway spruce stand. *Soil Biol. Biochem.* 39, 2103-2110.

801 Ekblad, A., Högberg, P., 2001. Natural abundance of ¹³C in CO₂ respired from forest soils
802 reveals speed of link between tree photosynthesis and root respiration. *Oecologia* 127, 305-
803 308.

804 Ekblad, A., Boström, B., Holm, A., Comstedt, D., 2005. Forest soil respiration rate and δ¹³C is
805 regulated by recent above ground weather conditions. *Oecologia* 143, 136-142.

806 Faimon, J., Troppová, D., Baldík, V., Novotný, R., 2012. Air circulation and its impact on
807 microclimatic variables in the Císařská Cave (Moravian Karst, Czech Republic). *Int. J. Climatol.*
808 32, 599-623.

809 Fang, C., Moncrieff, J.B., 2001. The dependence of soil CO₂ efflux on temperature. *Soil Biol.*
810 *Biochem.*, 33, 155-165.

811 Farquhar, G., O'Leary, M., Berry, J., 1982. On the Relationship Between Carbon Isotope
812 Discrimination and the Intercellular Carbon Dioxide Concentration in Leaves. *Funct. Plant Biol.*
813 9, 121-137.

814 Fernandez-Cortes, A., Sanchez-Moral, S., Cuezva, S., Cañaveras, J.C., Abella, R., 2009. Annual
815 and transient signatures of gas exchange and transport in the Castañar de Ibor cave (Spain).
816 *Int. J. Speleol.* 38, 153-162.

817 [Fernandez-Cortes, A., Sanchez-Moral, S., Cañaveras, J.C., Cuevas-Gonzalez, J., Cuezva, S.,](#)
818 [Andreu, J.M., 2010. Variations in seepage water geochemistry induced by natural and](#)
819 [anthropogenic microclimatic changes: Implications for speleothem growth conditions,](#)
820 [Geodinamica Acta. Taylor & Francis, pp. 1-13.](#)

821 Fernandez-Cortes, A., Sanchez-Moral, S., Cuezva, S. Benavente, D. and Abella, R., 2011.
822 Characterization of trace gases' fluctuations on a 'low energy' cave (Castañar de Íbor, Spain)
823 using techniques of entropy of curves. *Int. J. Climatol.* 31, 127-143.

824 Fernandez-Cortes, A., Benavente, D., Cuezva, S., Cañaveras, J.C., Alvarez-Gallego, M., Garcia-
825 Anton, E., Soler, V., Sanchez-Moral, S., 2013. Effect of water vapour condensation on the radon
826 content in subsurface air in a hypogeal inactive-volcanic environment in Galdar cave, Spain.
827 *Atmos. Environ.* 75, 15-23.

828 Fernandez-Cortes, A., Cuezva, S., Garcia-Anton, E., Alvarez-Gallego, M., Pla, C., Benavente, D.,
829 Cañaveras, J.C., Calaforra, J.M., Matthey, D.P., Sanchez-Moral, S., 2015a. Changes in the storage
830 and sink of carbon dioxide in subsurface atmospheres controlled by climate-driven processes:
831 the case of the Ojo Guareña karst system. *Environ. Earth Sci* 74, 7715-7730.

832 Fernandez-Cortes, A., Cuezva, S., Alvarez-Gallego, M., Garcia-Anton, E., Pla, C., Benavente, D.,
833 Jurado, V., Saiz-Jimenez, C., Sanchez-Moral, S., 2015b. Subterranean atmospheres may act as
834 daily methane sinks. *Nature Commun.* 6, 7003.

835 [Fisher, R., Lowry, D., Wilkin, O., Sriskantharajah, S., Nisbet, E. G., 2006. High-precision,](#)
836 [automated stable isotope analysis of atmospheric methane and carbon dioxide using](#)
837 [continuous-flow isotope-ratio mass spectrometry, Rapid Commun. Mass Sp., 20, 200-208.](#)

838 Frank, D.A., Reichstein, M., Bahn, M., Thonicke, K., Frank, D., Mahecha, M.D., Smith, P., Van
839 der Velde, M., Vicca, S., Babst, F., Beer, C., Buchmann, N., Canadell, J.G., Ciais, P., Cramer, W.,
840 Ibrom, A., Miglietta, F., Poulter, B., Rammig, A., Seneviratne, S.I., Walz, A., Wattenbach, M.,

841 Zavala, M.A., Zscheischler, J., 2015. Effects of climate extremes on the terrestrial carbon cycle:
842 concepts, processes and potential future impacts. *Glob. Change Biol.* 21, 2861-2880.

843 Frisia, S., Fairchild, I.J., Fohlmeister, J., Miorandi, R., Spoetl, C., Borsato, A., 2011. Carbon mass-
844 balance modelling and carbon isotope exchange processes in dynamic caves. *Geochim.*
845 *Cosmochim. Acta* 75, 380-400.

846 Garcia-Anton, E., Cuezva, S., Fernandez-Cortes, A., Benavente, D., Sanchez-Moral, S., 2014b.
847 Main drivers of diffusive and advective processes of CO₂-gas exchange between a shallow
848 vadose zone and the atmosphere. *Int. J. Greenh. Gas Con.* 21, 113-129.

849 Garcia-Anton, E., 2014b. Aplicación de la señal isotópica $\delta^{13}\text{CO}_2$ para la caracterización de
850 mecanismos de transporte de CO₂-gas entre atmósfera y subsuelo en sistemas kársticos
851 someros (Cueva de Altamira, Cantabria). University of Alicante, Alicante, p. 170.

852 Garcia-Guinea, J., Fernandez-Cortes, A., Alvarez-Gallego, M., Garcia-Antón, E., Casas-Ruiz, M.,
853 Blázquez-Pérez, D., Teijón, O., Cuezva, S., Correcher, V., Sanchez-Moral, S., 2013. Leaching of
854 uranyl-silica complexes from the host metapelite rock favoring high radon activity of subsoil
855 air: case of Castañar cave (Spain). *J. Radioanal. Nucl. Chem.* 298, 1567-1585.

856 Genty, D., 2008. Palaeoclimate research in Villars Cave (Dordogne, SW-France). *Int. J. Speleol.*
857 37, 3.

858 Gilfillan, S.M., Lollar, B.S., Holland, G., Blagburn, D., Stevens, S., Schoell, M., Cassidy, M., Ding,
859 Z., Zhou, Z., Lacrampe-Couloume, G., 2009. Solubility trapping in formation water as dominant
860 CO₂ sink in natural gas fields. *Nature* 458, 614-618.

861 Goffin, S., Aubinet, M., Maier, M., Plain, C., Schack-Kirchner, H., Longdoz, B., 2014.
862 Characterization of the soil CO₂ production and its carbon isotope composition in forest soil
863 layers using the flux-gradient approach. *Agr. Forest Meteorol.* 188, 45-57.

864 Grupo Espeleológico Edelweiss (1986) Complejo kárstico de Ojo Guareña. In: Diputación
865 Provincial de Burgos (Ed) Kaite, vol 4-5. Diputación Provincial de Burgos, Burgos, Spain.

866 Hamerlynck, E.P., Scott, R.L., Sánchez-Cañete, E.P., Barron-Gafford, G.A., 2013. Nocturnal soil
867 CO₂ uptake and its relationship to subsurface soil and ecosystem carbon fluxes in a Chihuahuan
868 Desert shrubland. *J. Geophys. Res. Biogeo.* 118, 2013JG002495.

869 Hashimoto, S., Komatsu, H., 2006. Relationships between soil CO₂ concentration and CO₂
870 production, temperature, water content, and gas diffusivity: implications for field studies
871 through sensitivity analyses. *J. For. Res.* 11, 41-50.

872 Hemming, D., Yakir, D., Ambus, P., Aurela, M., Besson, C., Black, K., Buchmann, N., Burlett, R.,
873 Cescatti, A., Clement, R., Gross, P., Granier, A., Grünwald, T., Havrankova, K., Janous, D.,
874 Janssens, I.A., Knohl, A., Östner, B.K., Kowalski, A., Laurila, T., Mata, C., Marcolla, B., Matteucci,
875 G., Moncrieff, J., Moors, E.J., Osborne, B., Pereira, J.S., Pihlatie, M., Pilegaard, K., Ponti, F.,
876 Rosova, Z., Rossi, F., Scartazza, A., Vesala, T., 2005. Pan-European $\delta^{13}\text{C}$ values of air and organic
877 matter from forest ecosystems. *Glob. Change Biol.* 11, 1065-1093.

878 Jabro, J.D., Sainju, U.M., Stevens, W.B., Evans, R.G., 2012. Estimation of CO₂ diffusion
879 coefficient at 0-10 cm depth in undisturbed and tilled soils. *Arch. Agron. Soil Sci.* 58, 1-9.

880 James, E.W., Banner, J.L., Hardt, B., 2015. A global model for cave ventilation and seasonal bias
881 in speleothem paleoclimate records. *Geochem. Geophys. Geosy.* 16, 1044-1051.

882 Jassal, R.S., Black, T.A., Cai, T., Morgenstern, K., Li, Z., Gaumont-Guay, D., Nesic, Z., 2007.
883 Components of ecosystem respiration and an estimate of net primary productivity of an
884 intermediate-aged Douglas-fir stand. *Agr. Forest Meteorol.* 144, 44-57.

885 Kayler, Z.E., Ganio, L., Hauck, M., Pypker, T.G., Sulzman, E.W., Mix, A.C., Bond, B.J., 2010. Bias
886 and uncertainty of $\delta(\text{CO}_2)\text{-C-13}$ isotopic mixing models. *Oecologia* 163, 227-234.

887 Keeling, C.D., 1958. The concentration and isotopic abundances of atmospheric carbon dioxide
888 in rural areas. *Geochim. Cosmochim. Acta* 13, 322-334.

889 Keeling, C.D., 1961. The concentration and isotopic abundances of carbon dioxide in rural and
890 marine air. *Geochim. Cosmochim. Acta* 24, 277-298.

891 Kowalski, A.S., Serrano-Ortiz, P., Janssens, I.A., Sánchez-Moral, S., Cuezva, S., Domingo, F.,
892 Were, A., Alados-Arboledas, L., 2008. Can flux tower research neglect geochemical CO₂
893 exchange? *Agr. Forest Meteorol.* 148, 1045-1054.

894 Lalueza-Fox, C., Rosas, A., Estalrrich, A., Gigli, E., Campos, P.F., Garcia-Tabernero, A., Garcia-
895 Vargas, S., Sanchez-Quinto, F., Ramirez, O., Civit, S., Bastir, M., Huguet, R., Santamaria, D.,
896 Gilbert, M.T.P., Willerslev, E., de la Rasilla, M., 2011. Genetic evidence for patrilocal mating
897 behavior among Neandertal groups. *P. Natl. Acad. Sci. U.S.A.* 108, 250-253.

898 Lario, J., Sanchez-Moral, S., Cuezva, S., Taborda, M., Soler, V., 2006. High Rn-222 levels in a
899 show cave (Castanar de Ibor, Spain): Proposal and application of management measures to
900 minimize the effects on guides and visitors. *Atmos. Environ.* 40, 7395-7400.

901 Liu, Z., Zhao, J., 2000. Contribution of carbonate rock weathering to the atmospheric CO₂ sink.
902 *Environ. Geol.* 39, 1053-1058.

903 Lloyd, J., Taylor, J.A., 1994. On the temperature-dependence of soil respiration. *Funct. Ecol.* 8,
904 315-323.

905 Mangin, A., Andrieux, C., 1988. Infiltration et environnement souterrain, le rôle de l'eau sur les
906 paramètres climatiques. *Actes des journées Félix Trombe T1, Mémoires du Spéléo-Club de*
907 *Paris* 14, 78-95.

908 Marron, N., Plain, C., Longdoz, B., Epron, D., 2009. Seasonal and daily time course of the ¹³C
909 composition in soil CO₂ efflux recorded with a tunable diode laser spectrophotometer (TDLS).
910 Plant Soil 318, 137-151.

911 Maseyk, K., Wingate, L., Seibt, U., Ghashghaie, J., Bathellier, C., Almeida, P., de Vale, R.L.,
912 Pereira, J.S., Yakir, D., Mencuccini, M., 2009. Biotic and abiotic factors affecting the delta C-13
913 of soil respired CO₂ in a Mediterranean oak woodland. Isot. Environ. Healt. S. 45, 343-359.

914 Matthey, D.P., Fairchild, I.J., Atkinson, T.C., Latin, J.-P., Ainsworth, M., Durrell, R., 2010. Seasonal
915 microclimate control of calcite fabrics, stable isotopes and trace elements in modern
916 speleothem from St Michaels Cave, Gibraltar. Geol. Soc. Spec. Publ. 336, 323-344.

917 Matthey, D.P., Atkinson, T.C., Barker, J.A., Fisher, R., Latin, J.P., Durrell, R., Ainsworth, M., 2016.
918 Carbon dioxide, ground air and carbon cycling in Gibraltar karst. Geochim. Cosmochim. Acta
919 184, 88-113.

920 Morner, N.A., Etiope, G., 2002. Carbon degassing from the lithosphere. Global Planet. Change
921 33, 185-203.

922 Moyes, A.B., Gaines, S.J., Siegwolf, R.T.W., Bowling, D.R., 2010. Diffusive fractionation
923 complicates isotopic partitioning of autotrophic and heterotrophic sources of soil respiration.
924 Plant Cell Environ. 33, 1804-1819.

925 Nickerson, N., Risk, D., 2009. Physical controls on the isotopic composition of soil-respired CO₂.
926 J. Geophys. Res. Biogeo. 114, G01013.

927 Noronha, A.L., Johnson, K.R., Southon, J.R., Hu, C., Ruan, J., McCabe-Glynn, S., 2015.
928 Radiocarbon evidence for decomposition of aged organic matter in the vadose zone as the
929 main source of speleothem carbon. Quaternary Sci. Rev. 127, 37-47.

930 Pataki, D.E., Ehleringer, J.R., Flanagan, L.B., Yakir, D., Bowling, D.R., Still, C.J., Buchmann, N.,
931 Kaplan, J.O., Berry, J.A., 2003. The application and interpretation of Keeling plots in terrestrial
932 carbon cycle research. *Global Biogeochem. Cy.* 17, 1022.

933 Peña, J.A., 2011. Descripción física del complejo cárstico y sus conexiones exteriores, in: de la
934 Rasilla, M., Rosas, A., Cañaveras, J.C., Lalueza-Fox, C. (Eds.), *La cueva de El Sidrón (Borines,*
935 *Piloña, Asturias). Investigación interdisciplinar de un grupo neandertal. Conserjería de Cultura*
936 *y Turismo. Gobierno del Principado de Asturias, pp. 21-26.*

937 Pla, C., Cuezva, S., Garcia-Anton, E., Fernandez-Cortes, A., Cañaveras, J.C., Sanchez-Moral, S.,
938 Benavente, D., 2016. Changes in the CO₂ dynamics in near-surface cavities under a future
939 warming scenario: Factors and evidence from the field and experimental findings. *Sci. Total*
940 *Environ.*, 565, 1151-1164.

941 Pla, C., Cuezva, S., Martinez-Martinez, J., Fernandez-Cortes, A., Garcia-Anton, E., Fusi, N.,
942 Crosta, G.B., Cuevas-Gonzalez, J., Cañaveras, J.C., Sanchez-Moral, S., Benavente, D., 2017a.
943 Role of soil pore structure in water infiltration and CO₂ exchange between the atmosphere and
944 underground air in the vadose zone: A combined laboratory and field approach. *Catena* 149(1),
945 402-416.

946 Pla, C., 2017b. Modelización del transporte difusivo de gases en el conjunto suelo-roca.
947 Aplicación al análisis e interpretación de datos microclimáticos en sistemas kársticos someros.
948 Ph. D. Thesis, Universidad de Alicante, p. 217.

949 Richon, P., Perrier, F., Koirala, B.P., Girault, F., Bhattarai, M., Sapkota, S.N., 2011. Temporal
950 signatures of advective versus diffusive radon transport at a geothermal zone in Central Nepal.
951 *J. Environ. Radioactiv.* 102, 88-102.

952 Risk, D., Kellman, L., Beltrami, H., 2002. Carbon dioxide in soil profiles: Production and
953 temperature dependence. *Geophys. Res. Lett.* 29, 11-11-11-14.

954 Risk, D., Kellman, L., 2008. Isotopic fractionation in non-equilibrium diffusive environments.
955 Geophys. Res. Lett. 35, L02403.

956 Roland, M., Serrano-Ortiz, P., Kowalski, A.S., Godd ris, Y., S nchez-Ca nete, E.P., Ciais, P.,
957 Domingo, F., Cuezva, S., Sanchez-Moral, S., Longdoz, B., Yakir, D., Van Grieken, R., Schott, J.,
958 Cardell, C., Janssens, I.A., 2013. Atmospheric turbulence triggers pronounced diel pattern in
959 karst carbonate geochemistry. Biogeo. 10, 5009-5017.

960 Rosas, A., Mart nez-Maza, C., Bastir, M., Garc a-Tabernero, A., Lalueza-Fox, C., Huguet, R.,
961 Ortiz, J.E., Juli , R., Soler, V., De Torres, T., Mart nez, E., Ca averas, J.C., S nchez-Moral, S.,
962 Cuezva, S., Lario, J., Santamar a, D., De La Rasilla, M., Fortea, J., 2006. Paleobiology and
963 comparative morphology of a late Neandertal sample from El Sidr n, Asturias, Spain. P. Natl.
964 Acad. Sci. U.S.A. 103, 19266-19271.

965 Ryan, M.G., Law, B.E., 2005. Interpreting, measuring, and modeling soil respiration.
966 Biogeochemistry 73, 3-27.

967 Sanchez-Ca nete, E.P., Serrano-Ortiz, P., Kowalski, A.S., Oyonarte, C., Domingo, F., 2011.
968 Subterranean CO₂ ventilation and its role in the net ecosystem carbon balance of a karstic
969 shrubland. Geophys. Res. Lett. 38, L09802.

970 Sanchez-Ca nete, E.P., Serrano-Ortiz, P., Domingo, F., Kowalski, A.S., 2013. Cave ventilation is
971 influenced by variations in the CO₂-dependent virtual temperature. Int. J. Speleol. 42, 1-8.

972 Sanchez-Moral, S., Soler, V., Canaveras, J.C., Sanz-Rubio, E., Van Grieken, R., Gysels, K., 1999.
973 Inorganic deterioration affecting the Altamira Cave, N Spain: quantitative approach to wall-
974 corrosion (solutional etching) processes induced by visitors. Sci. Total Environ. 243/244, 67-84.

975 Serrano-Ortiz, P., Roland, M., Sanchez-Moral, S., Janssens, I.A., Domingo, F., Godderis, Y.,
976 Kowalski, A.S., 2010. Hidden, abiotic CO₂ flows and gaseous reservoirs in the terrestrial carbon
977 cycle: Review and perspectives *Agr. Forest Meteorol.* 151, 529-529.

978 Schwalm, C.R., Williams, C.A., Schaefer, K., Baldocchi, D., Black, T.A., Goldstein, A.H., Law, B.E.,
979 Oechel, W.C., Paw U, K.T., Scott, R.L., 2012. Reduction in carbon uptake during turn of the
980 century drought in western North America. *Nature Geosci.* 5, 551-556.

981 Shanhun, F.L., Almond, P.C., Clough, T.J., Smith, C.M.S., 2012. Abiotic processes dominate CO₂
982 fluxes in Antarctic soils. *Soil Biol. Biochem.* 53, 99-111.

983 Spotl, C., Fairchild, I.J., Tooth, A.F., 2005. Cave air control on dripwater geochemistry, Obir
984 Caves (Austria): Implications for speleothem deposition in dynamically ventilated caves.
985 *Geochim. Cosmochim. Acta* 69, 2451-2468.

986 Vaughn, B., Evans, C., White, J.C., Still, C., Masarie, K., Turnbull, J., 2010. Global Network
987 Measurements of Atmospheric Trace Gas Isotopes, in: West, J.B., Bowen, G.J., Dawson, T.E.,
988 Tu, K.P. (Eds.), *Isoscapes: Understanding Movement, Pattern, and Process on Earth Through*
989 *Isotope Mapping*. Springer Netherlands, pp. 3-31.

990 Vicca, S., Bahn, M., Estiarte, M., van Loon, E., Vargas, R., Alberti, G., Ambus, P., Arain, M., Beier,
991 C., Bentley, L., 2014. Can current moisture responses predict soil CO₂ efflux under altered
992 precipitation regimes? A synthesis of manipulation experiments. *Biogeosciences Discuss.* 11,
993 2991-3013.

994 Wang, W., Chen, X., Luo, G., Li, L., 2014. Modeling the contribution of abiotic exchange to CO₂
995 flux in alkaline soils of arid areas. *J. Arid Land* 6, 27-36.

996 Xu, L., Baldocchi, D.D., Tang, J., 2004. How soil moisture, rain pulses, and growth alter the
997 response of ecosystem respiration to temperature. *Global Biogeochem. Cy.* 18, GB4002.

- 998 Yakir, D., Sternberg, L.D.L., 2000. The use of stable isotopes to study ecosystem gas exchange.
999 *Oecologia* 123, 297-311.
- 1000 Zobitz, J.M., Keener, J.P., Schnyder, H., Bowling, D.R., 2006. Sensitivity analysis and
1001 quantification of uncertainty for isotopic mixing relationships in carbon cycle research. *Agr.*
1002 *Forest Meteorol.* 136, 56-75.
- 1003

1004 **Figure captions**

1005 **Figure 1:** Diagram illustrating the main pathways of CO₂(g)-exchange between atmosphere, soil
1006 and the cave and major transport mechanisms between them (simplified from Matthey et al.,
1007 2016). The more complex set of processes related to vadose groundwater as vehicle of CO₂
1008 transport to cave atmosphere (i.e. the formation of carbonic acid in soil and epikarst zone,
1009 dissolution of bedrock and degassing of drip water), has been simplified in a singled process
1010 named as “Infiltrating water”. In addition, the term “Soil-derived CO₂” includes all CO₂
1011 originally generated within soil (roots respiration and soil organic matter degradation) and the
1012 subsequent process as direct gas diffusion mainly from deeper soil layer or previously
1013 accumulated in the fissures, fractures and pore-spaces of rock in the vadose zone and,
1014 additionally, the CO₂ derived from microbial oxidation of down-washed organic matter.

1015 **Figure 2:** Geographic and climatic locations of the studied caves. Climatic classification follows
1016 the Köppen-Geiger method with slight modifications (adapted from AEMET-IM, 2008). Letters
1017 B, C, D and E refers to Arid, Temperate, Continental and Polar climates. Study sites are located
1018 at temperate humid (Cfb) and temperate dry (Csa) climates also named Oceanic and
1019 Mediterranean respectively.

1020 **Figure 3:** A) Plan view of Altamira cave, B) Cross section of the cave.

1021 **Figure 4:** A) Plan view of Castañar cave with 5 cross sections, B) Galleries distributions in a SE-
1022 NW topography section following the maximum gradient line.

1023 **Figure 5:** A) Map of the cave sectors where the study has been carried out. B) Detailed cross-
1024 sections of the cave galleries in relation to surface geomorphology and the main entrances to
1025 the subterranean system (solid black line represents the studied galleries; the ends of these
1026 galleries continue with the rest of the subterranean system, which is not drawn; the dotted
1027 lines show the locations of other cave levels).

1028 **Figure 6:** A) Plan view of Rull cave, B) Cross section of the cave.

1029 **Figure 7:** A) Map of the El Sidron cave system, B) Cross section of the cave.

1030 **Figure 8:** Annual cycles of the main parameters registered in the Altamira, Castañar, Ojo
1031 Guareña and Rull caves. (A) monthly average temperature (circles) and total monthly rainfall
1032 (bars). (B) monthly average relative humidity in the air (triangles) and volumetric water
1033 content in the soil at 5 cm depth (circles). (C) monthly average radon concentration contained
1034 in the inner parts of the cave (squares). (D) mean values of CO₂ (squares) and $\delta^{13}\text{CO}_2$
1035 (diamonds) for each field campaign in the cave atmosphere. (E) mean values of CO₂ (hexagons)
1036 and $\delta^{13}\text{CO}_2$ (diamonds) for each field campaign in the soil air.(F) isotopic signal $\delta^{13}\text{C}$ of the
1037 source of CO₂ for the soil ($\delta^{13}\text{C}_s$ -soil, triangles) and the entire system ($\delta^{13}\text{C}_s$ -system, squares)
1038 estimated using the Keeling plot model (see text). Shaded area represents the warmer months
1039 of the represented annual cycles.

1040 **Figure 9:** Keeling plots of the total amount of samples collected in the soil (circles), cave
1041 (diamonds) and exterior air (squares) at each cave site.

1042 **Figure 10:** Keeling plots of the samples collected in different field campaigns at the Castañar de
1043 Ibor, Ojo Guareña, Rull and El Sidron caves. Different values of the intercept were obtained for
1044 the air contained in the soil ($\delta^{13}\text{C}_s$ -soil) and the entire system ($\delta^{13}\text{C}_s$ -system, see text).

1045 **Figure 11:** (A) Relationship between the average values $\delta^{13}\text{CO}_2$ and VWC at 5 cm depth
1046 (volumetric water content) and (B) the average values $\delta^{13}\text{CO}_2$ and CO₂ during each field
1047 campaign in the soil at Altamira (squares) and Castañar de Ibor (diamonds).

1048 **Figure 12:** Relationship between the average values of $\delta^{13}\text{C}_s$ -soil (isotopic ratio of the source of
1049 soil-contained CO₂ calculated from Keeling plot, see Fig. 10) and VWC (volumetric water
1050 content) at 5 cm depth at Altamira (squares) and Castañar de Ibor (diamonds).

1051 Figure 13: Keeling plot of $1/\text{CO}_2$ versus $\delta^{13}\text{CO}_2$ soil air (A) and cave air (B) for all samples
1052 collected in the 5 field sites. The dotted crosshairs correspond to the averaged composition of
1053 the 5 local atmospheres in this study. Solid squares: samples of background atmosphere, solid
1054 circles: soil air samples, and open rectangles: cave air samples. Each colour code corresponds
1055 to a single studied cave. Panel B: data points can be envisaged as representing mixtures (cave
1056 air) of average atmospheric air with a CO_2 -rich component derived from soil. The keeling plots
1057 for each cave site are plotted by coloured dashed lines, according to results from Fig.9. The
1058 thicker and continuous black line corresponds to the modelled mixing process between both
1059 components (see text for further details) and the perpendicular dotted lines are contours of
1060 equal mixing ratios labelled as % of remaining (soil-derived) CO_2 in the cave air. Data for New
1061 St. Michaels cave air (Mattey et al., 2016) is also plotted for comparison (grey crosses) and
1062 interpreted as a mix of atmosphere and ground air (grey shaded area and black straight line).
1063 See text for a detailed description of the modelled processes and further discussion.

1064 **Figure 14:** Linear correlation between the monthly average values of cave air ^{222}Rn and CO_2
1065 concentrations in Altamira, Castañar de Ibor, Ojo Guareña and Rull caves during the respective
1066 sampling periods.

1067 **Figure 15:** Relationship between $\delta^{13}\text{C}_s$ -system (isotopic ratio of the source of system CO_2
1068 calculated from the Keeling plot, see Fig. 10) and VWC at 5 cm depth during each field
1069 campaign in the soil at Altamira (squares) and Castañar de Ibor (diamonds).

1070

1071 **Table captions**

1072 **Table 1:** Data summary of the main features of the studied caves (extracted from Fernandez-
1073 Cortes et al., 2015b, supplementary information). A detailed description and additional data
1074 can be found in: 1) Cuezva et al., 2009 and Cuezva et al., 2011; 2) Fernandez-Cortes et al., 2011
1075 and Alonso-Zarza et al., 2011; 3) Camacho et al., 2006 and Fernandez-Cortes et al., 2015a; 4)
1076 Pla et al., 2015 and 5) Rosas et al., 2006 and Lalueza-Fox et al., 2011.

1077 **Table 2:** Average values and ranges of variation (difference between maximum and minimum
1078 values) for the CO₂ concentration and the $\delta^{13}\text{CO}_2$ in the air. Values have been grouped
1079 according to the air mass (soil, cave or exterior air), field campaign and study site. The isotopic
1080 ratio of the source ($\delta^{13}\text{C}_s$) is also referred. This was calculated with the Keeling model for the
1081 soil ($\delta^{13}\text{C}_s\text{-soil}$) and the system ($\delta^{13}\text{C}_s\text{-system}$) for each field campaign.

1082 **Table 3:** Mean values and ranges of variation for the total amount of samples collected during
1083 the annual cycles studied at each field site.

Table 1

[Click here to download Table: Table_1.doc](#)

Cave	Geographic coordinates of cave entrance			Host-rock	Morphometric data			Climate: average annual data			
	latitude	longitude	altitude (m.a.s.l.)		Depth of the sampled area	Length of the sampled area	Total length	Classification	T (°C)	Rain (mm)	Cave T (°C)
Altamira ¹	43° 22' 40" N	4° 7' 6" W	159	Dolomitized calcarenitic limestones	3 – 22 m (average 8 m)	220 m	270 m	Oceanic or Cfb: temperate without dry season and temperate summer	13.9	1350	13.7
Castañar de Ibor ²	39° 38' 13" N	5° 25' 33" W	590	Shales and greywackes with dolostones	15 – 55 m (average 25 m)	650 m	2315 m	Mediterranean or Csa: temperate with dry and hot summer	15.5	546	17.0
Ojo Guareña ³	42° 02' N	3° 39' W	785	Limestones and dolomitic limestones	30 -80 m (average 52 m)	2.5 Km	110 Km	Oceanic or Cfb: temperate without dry season and temperate summer	10.1	778.1	10.8
Rull ⁴	38° 48' 20" N	0° 10' 38" W	490	Limestone conglomerates	9 - 23 m (average 18 m)	46 m	46 m	Mediterranean or Csa: temperate with dry and hot summer	15.8	319	15.9
El Sidron ⁵	43° 23'07" N	5° 19' 34" W	167	Limestone conglomerates and sandstones	5 - 35 m (average 23 m)	600 m	600 m	Oceanic or Cfb: temperate without dry season and temperate summer	13.1	1292	12.0

Table 2
[Click here to download Table: Table_2.doc](#)

Location	Date	Soil					Cave					Exterior					$\delta^{13}\text{Cs}$	
		CO_2 (ppm)		$\delta^{13}\text{CO}_2$ (‰)		N	CO_2 (ppm)		$\delta^{13}\text{CO}_2$ (‰)		N	CO_2 (ppm)		$\delta^{13}\text{CO}_2$ (‰)		N	Keeling plot intercept	
		Average	Range	Average	Range		Average	Range	Average	Range		Average	Range	system	soil			
Altamira	Sep-11	5163.6	2335.0	-25.8	0.6	6	2163.0	2845.3	-23.7	4.3	15	420.5	97.5	-11.3	3.6	5	-27.0	-27.1
	Nov-11	4015.3	4184.0	-27.2	3.8	7	5678.0	2001.0	-26.2	0.5	19	436.1	23.9	-12.5	1.5	5	-27.8	-29.4
	Jan-12	2978.9	1242.6	-25.5	2.9	8	4151.4	1540.9	-26.1	0.9	11	424.6	8.5	-11.0	3.6	5	-27.9	-28.0
	Mar-12	5084.2	3199.9	-26.7	1.9	7	3320.8	656.4	-26.4	0.6	16	412.7	23.4	-11.6	2.9	9	-28.4	-28.2
	May-12	2434.7	898.8	-24.3	1.6	8	4727.2	942.2	-26.3	0.9	9	426.0	49.4	-9.7	2.3	11	-27.7	-27.5
	Jul-12	1213.9	1020.6	-20.6	3.9	8	1277.4	1727.1	-21.8	7.1	23	435.1	54.4	-10.4	2.5	7	-27.5	-26.3
	Sep-12	935.5	96.5	-19.6	1.5	14	1518.9	1855.7	-22.2	7.8	24	434.7	30.7	-11.3	1.9	13	-27.1	-26.7
Castañar de Ibor	Sep-11	2012.6	75.8	-20.5	0.5	2	3933.1	151.6	-23.7	0.2	5	411.3	20.8	-10.7	1.8	2	-24.7	-23.0
	Oct-11	1192.9	227.5	-19.2	1.1	4	3874.0	172.1	-24.0	0.4	11	468.2		-12.1		1	-25.5	-23.9
	Nov-11	6981.7	4889.3	-26.7	2.5	8	4341.1	286.5	-24.0	0.8	12	444.7	48.7	-12.6	2.1	2	-26.3	-27.7
	Dec-11	5595.1	1335.5	-26.4	2.2	15	4457.6	237.2	-24.4	0.5	12	437.2	18.0	-10.3	0.2	3	-27.0	-27.8
	Jan-12	3312.0	663.7	-24.9	2.6	10	3985.8	469.9	-24.2	1.1	12	464.0	64.4	-11.7	0.5	2	-26.3	-27.0
	Feb-12	3036.1	682.1	-24.2	1.9	8	3387.7	491.2	-24.8	0.5	12	410.6	7.8	-11.6	1.2	3	-26.4	-26.2
	Mar-12	3859.3	1120.5	-22.4	1.2	6	3291.4	139.4	-24.4	0.8	11	423.6	38.5	-11.4	1.9	6	-25.4	-23.8
	Apr-12	7445.1	544.3	-24.2	1.4	8	3565.5	121.5	-24.4	1.3	10	438.0	29.6	-10.4	1.1	4	-25.7	-25.1
	May-12	8116.1	1725.4	-24.4	1.3	12	3466.2	252.9	-24.8	0.5	12	435.8	53.7	-11.3	2.0	10	-25.9	-25.2
	Jun-12	2834.1	141.8	-20.9	1.4	7	3663.1	302.1	-24.9	1.7	12	428.6	12.0	-11.9	0.7	4	-25.2	-22.5
	Jul-12	2029.0	369.8	-19.2	0.3	4	3493.3	868.5	-24.5	0.8	12	418.4	3.6	-10.3	1.0	4	-25.5	-21.5
	Aug-12	1621.8	125.3	-19.1	0.5	8	2765.2	888.2	-23.5	3.0	11	438.0	17.2	-10.7	0.4	5	-24.7	-22.6
	Sep-12	1139.5	110.3	-18.8	0.9	5	2750.5	533.1	-23.9	3.1	12	457.3	75.2	-11.6	2.5	7	-25.9	-24.4
Ojo Guareña	Jun-13	3119.1	1986.1	-23.6	1.9	6	538.8	304.8	-15.4	9.9	14	399.1	6.9	-9.8	0.9	4	-26.6	-25.8
	Sep-13	6524.3	2393.6	-24.8	0.6	5	989.1	2361.4	-18.2	15.2	15	411.6	15.7	-8.4	0.0	2	-26.6	-26.0
	Oct-13	3276.5	1568.8	-23.8	1.3	6	601.7	748.4	-15.4	11.7	15	407.3	35.8	-9.1	1.7	5	-26.6	-25.9
	Dec-13	6330.2	5852.0	-25.7	2.3	8	457.7	116.9	-12.1	5.3	17	440.5	31.5	-11.4	1.2	6	-27.1	-27.1
	Feb-14	4234.8	2435.5	-26.3	2.8	8	496.8	485.4	-12.3	10.5	15	417.3	14.7	-9.8	1.0	6	-28.3	-28.2
	Apr-14	5543.6	3332.1	-25.6	1.4	8	502.2	144.4	-13.0	7.6	15	423.7	37.8	-9.4	1.7	6	-27.1	-26.9
Rull	Jun-14	6370.7	7469.9	-23.6	3.7	8	1023.3	2074.7	-17.6	15.8	16	422.2	37.4	-8.2	1.7	6	-25.9	-25.3
	Jan-14	2023.4	436.6	-24.3	1.1	6	892.0	54.6	-20.7	0.5	13	414.0	16.8	-9.4	1.8	7	-29.1	-28.2
	Feb-14	1586.7	860.3	-22.4	2.0	4	814.4	82.0	-19.6	1.5	7	421.0	37.4	-9.3	1.6	4	-28.6	-27.6
	Mar-14	1925.9	926.6	-23.0	1.0	3	964.2	48.5	-19.8	0.8	5	429.2	5.1	-8.9	0.7	3	-27.7	-27.2
	Apr-14	2654.3	262.1	-23.3	0.5	4	2453.2	52.9	-23.9	0.6	5	427.2	14.4	-9.3	1.5	3	-26.6	-26.0
	Jul-14	1350.8	235.6	-19.2	0.2	4	2376.9	416.0	-23.9	0.7	6	433.4	37.7	-9.1	1.1	3	-26.3	-23.9
	Aug-14	968.5	491.2	-17.0	3.0	4	2777.6	505.2	-24.7	1.0	6	417.4	20.0	-8.2	2.4	3	-27.0	-24.1
	Sep-14	1045.9	252.5	-17.7	1.1	4	2890.2	959.6	-24.2	2.2	7	438.7	15.1	-8.7	0.4	3	-26.6	-24.3
	Oct-14	2622.5	1606.7	-23.9	2.4	4	1949.0	868.1	-23.3	3.5	7	430.9	32.9	-10.3	2.3	3	-27.0	-26.9
	Nov-14	1473.7	386.5	-22.9	1.3	4	1230.5	202.7	-22.0	2.1	7	413.2	14.1	-9.6	1.0	3	-28.2	-28.1
	Dec-14	1352.4	760.6	-23.2	3.8	4	1033.7	41.4	-21.8	0.4	7	423.2	13.5	-10.7	0.8	3	-29.5	-29.4
El Sidron	Jan-15	1393.4	685.8	-23.5	2.0	3	869.8	84.1	-21.0	0.9	6	440.3	34.4	-11.7	2.7	3	-29.8	-29.3
	Sep-11	4528.2	1665.9	-26.1	2.3	6	1368.5	2444.5	-20.9	9.0	11	445.2	48.0	-12.5	2.9	3	-27.4	-27.6
	Jan-12	2183.4	494.6	-25.0	1.2	4	552.9	114.1	-16.2	3.8	14	476.4	13.7	-13.8	0.4	3	-28.1	-28.1
	Jul-12	2150.4	2293.3	-24.3	3.0	7	941.4	456.1	-19.4	4.6	13	432.6	17.2	-10.2	0.7	3	-28.1	-28.2

Table 3
[Click here to download Table: Table_3.doc](#)

Location	Sampling period	Soil					Cave					Exterior				
		CO ₂ (ppm)		δ ¹³ CO ₂ (‰)		N	CO ₂ (ppm)		δ ¹³ CO ₂ (‰)		N	CO ₂ (ppm)		δ ¹³ CO ₂ (‰)		N
		Average	Range	Average	Range		Average	Range	Average	Range		Average	Range	Average	Range	
Altamira	sept 2011-sept2012	2773.2	5686.8	-23.6	9.9	58	2969.5	5566.8	-24.2	9.7	117	427.2	97.5	-11.0	4.4	55
Castañar de Ibor	sept 2011-sept 2012	4461.0	8374.9	-23.3	9.8	97	3604.9	2537.2	-24.3	4.3	144	435.5	99.7	-11.2	3.9	53
Ojo Guareña	jun 2013-jun 2014	5119.0	7528.9	-24.9	6.3	49	659.3	2368.6	-14.8	16.5	107	419.4	66.3	-9.5	4.8	35
Rull	jan 2014-jan 2015	1689.0	2854.4	-21.9	10.2	44	1582.3	2330.4	-22.1	6.0	76	424.8	51.8	-9.5	5.9	38
El Sidron	sept 2011-jul 2012	2997.4	3616.2	-25.1	3.8	17	921.9	2492.5	-18.7	9.9	38	451.4	68.3	-12.1	4.1	9

Figure 1
[Click here to download high resolution image](#)

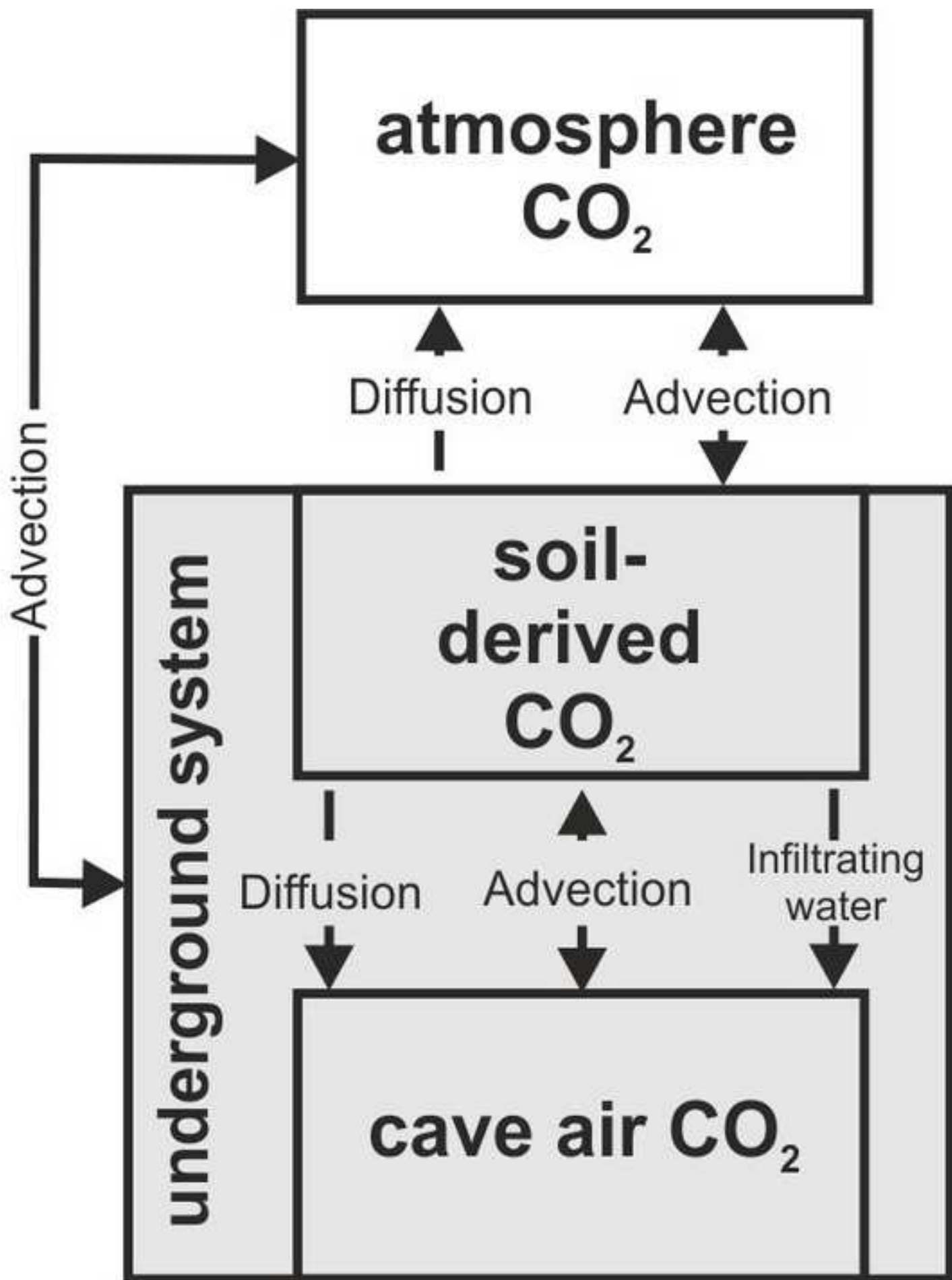
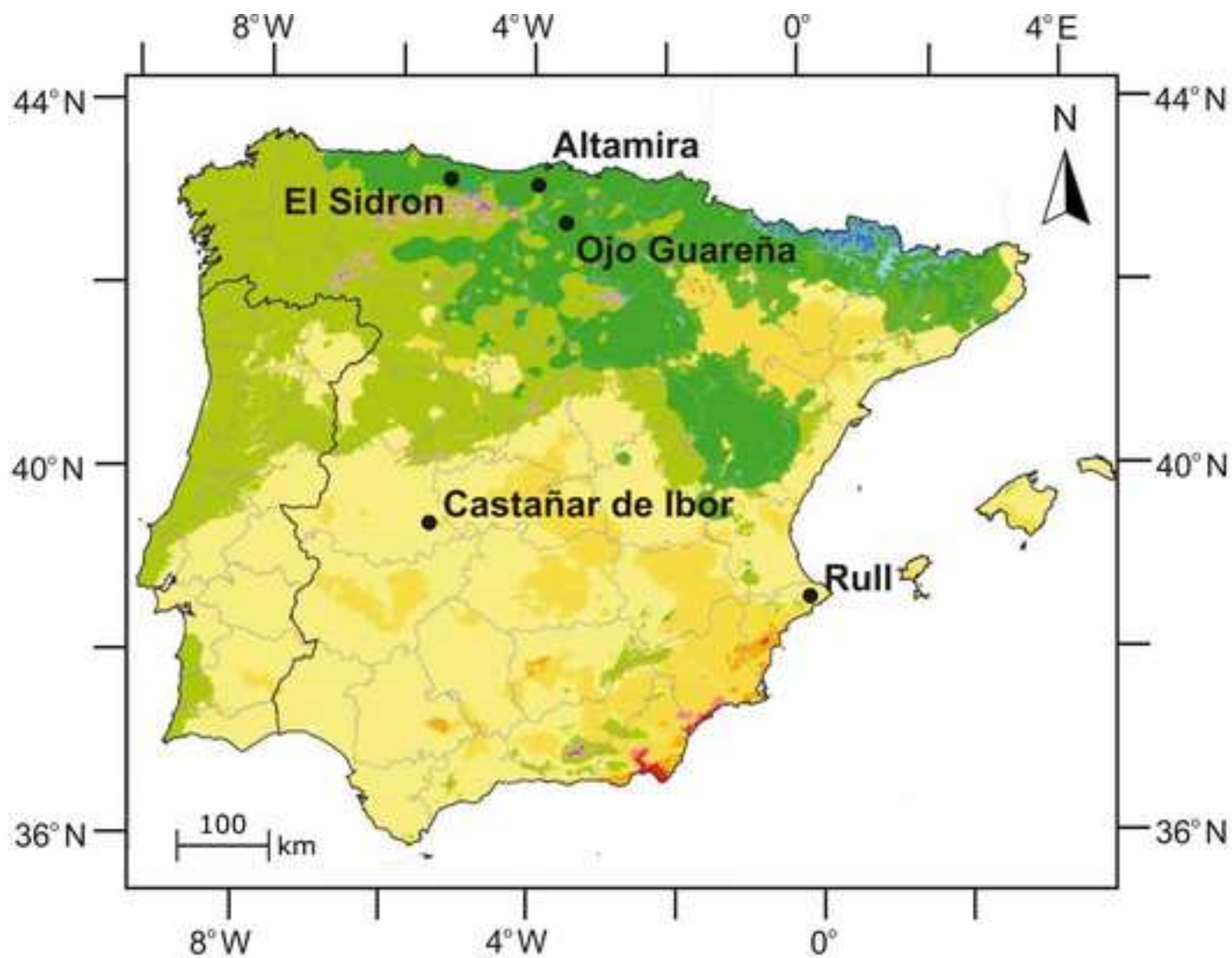


Figure 2

[Click here to download high resolution image](#)



LEGEND

-  BWh: hot desert
-  BWh: cold desert
-  BSh: hot steepe
-  BSk: cold steepe
-  Csa: temperate with dry and hot summer
-  Csb: temperate with dry and temperate summer
-  Cfa: temperate without dry season and hot summer
-  Cfb: temperate without dry season and temperate summer
-  Dsb: cold with dry and temperate summer
-  Dsc: cold with dry and fresh summer
-  Dfb: cold without dry season and temperate summer
-  Dfc: cold with a dry season and fresh summer
-  ET: tundra

Figure 3
[Click here to download high resolution image](#)

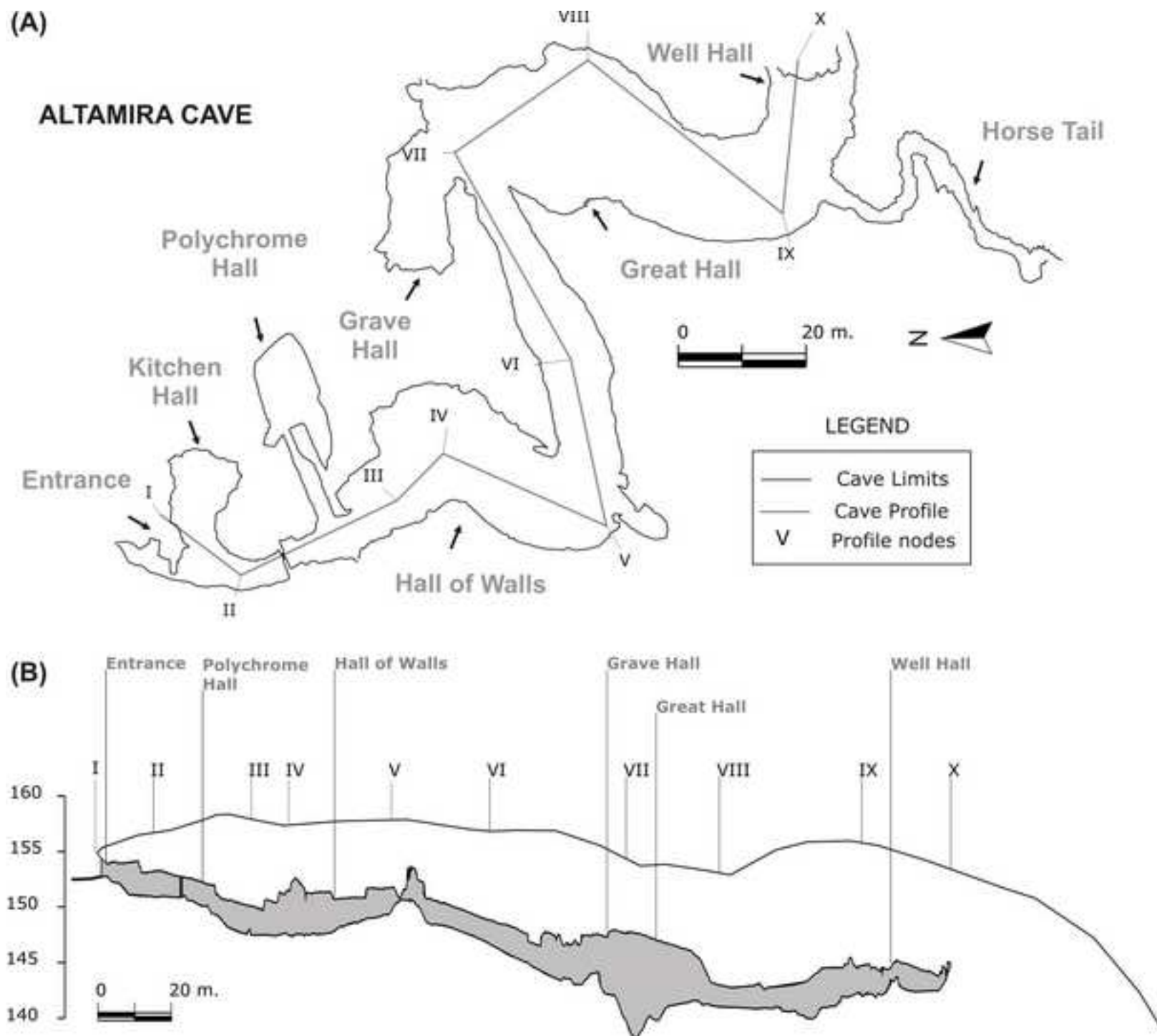


Figure 4
[Click here to download high resolution image](#)

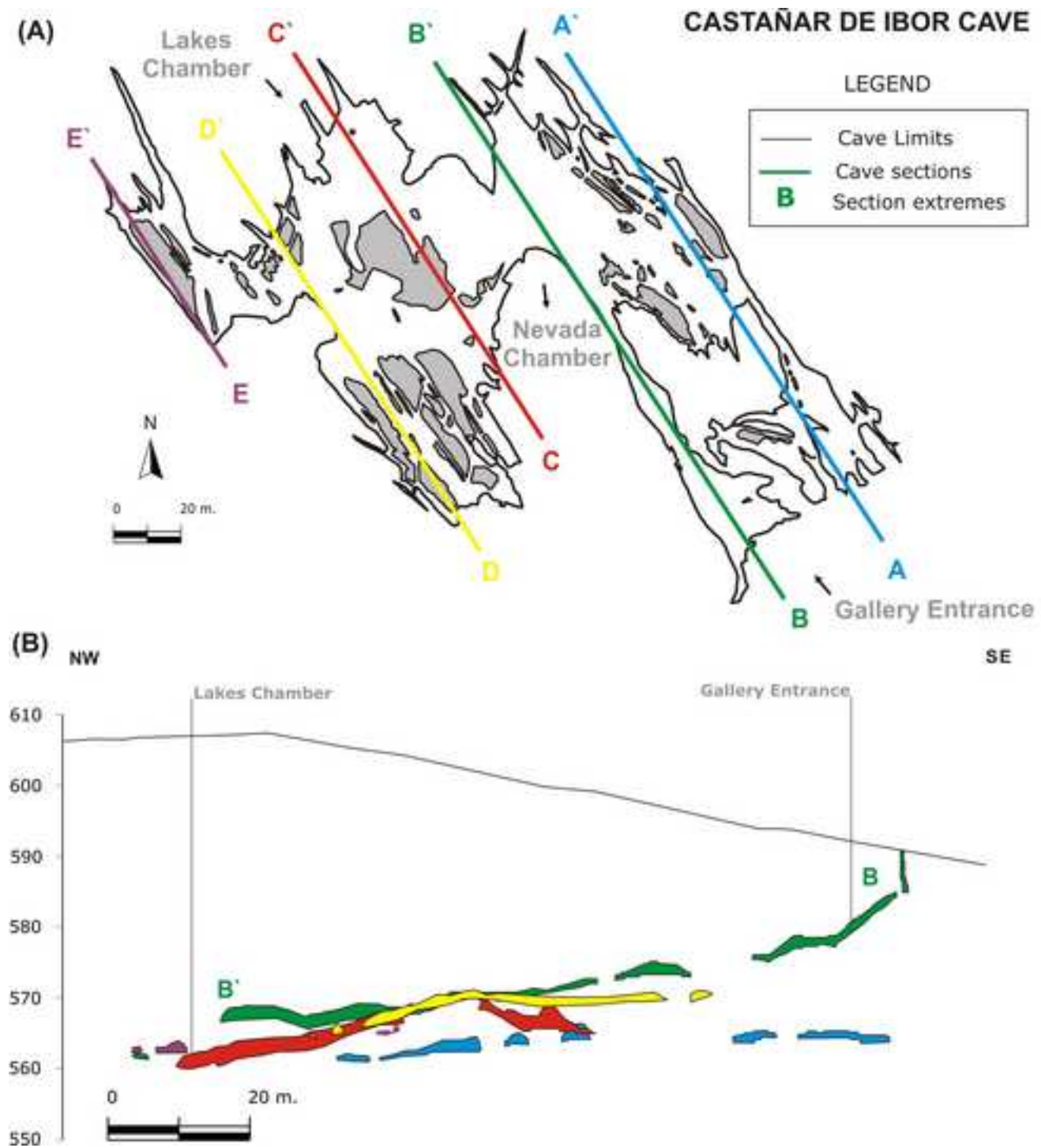


Figure 5
[Click here to download high resolution image](#)

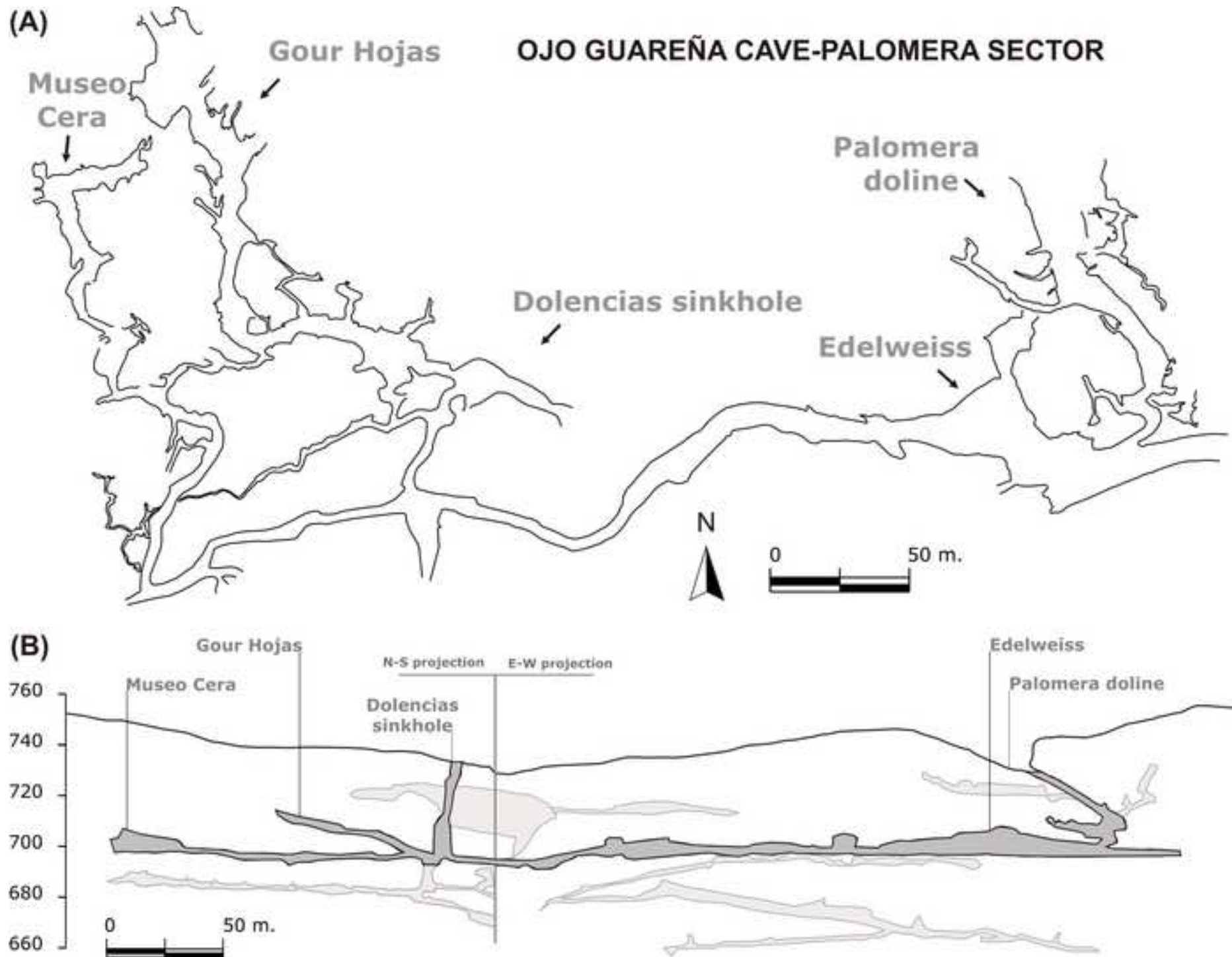


Figure 6
[Click here to download high resolution image](#)

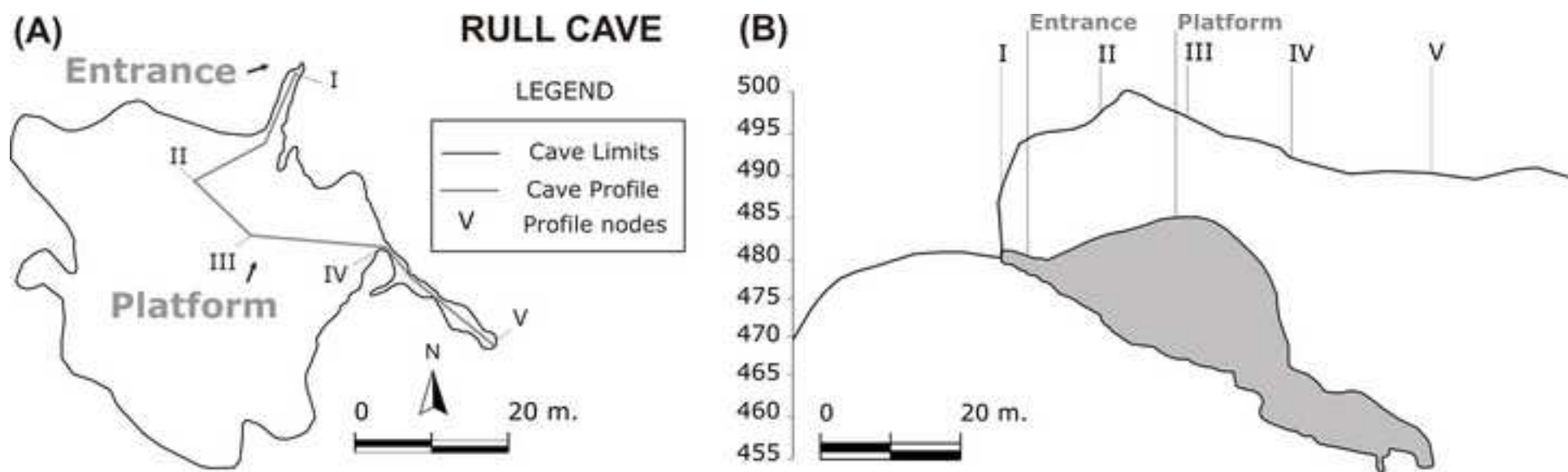


Figure 7
[Click here to download high resolution image](#)

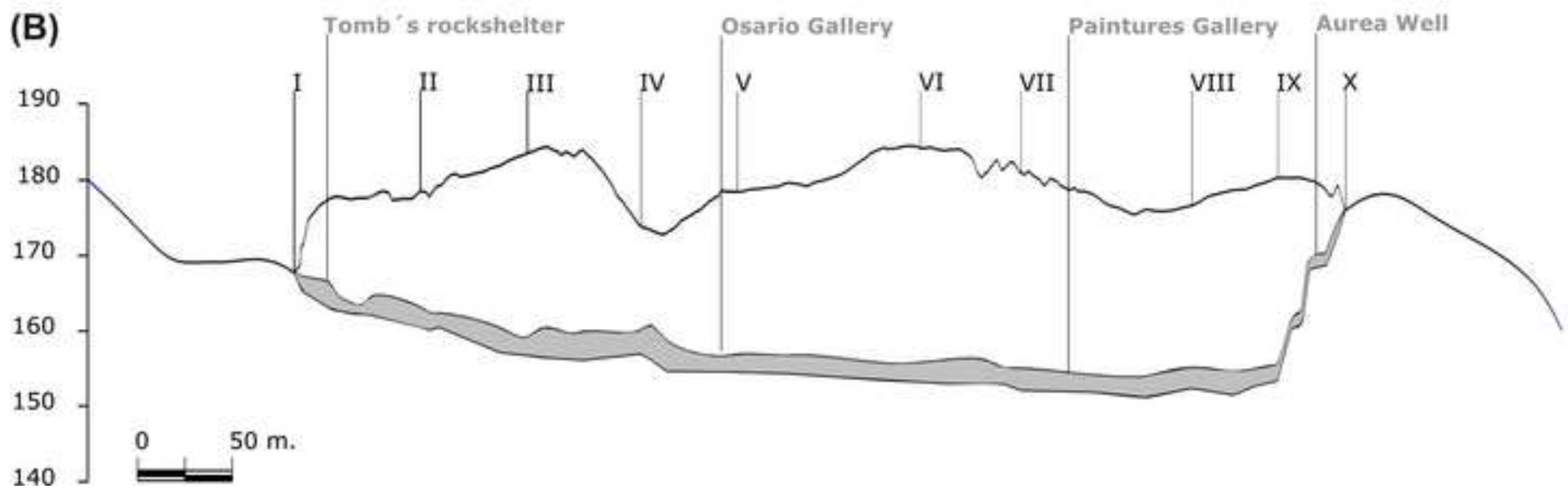
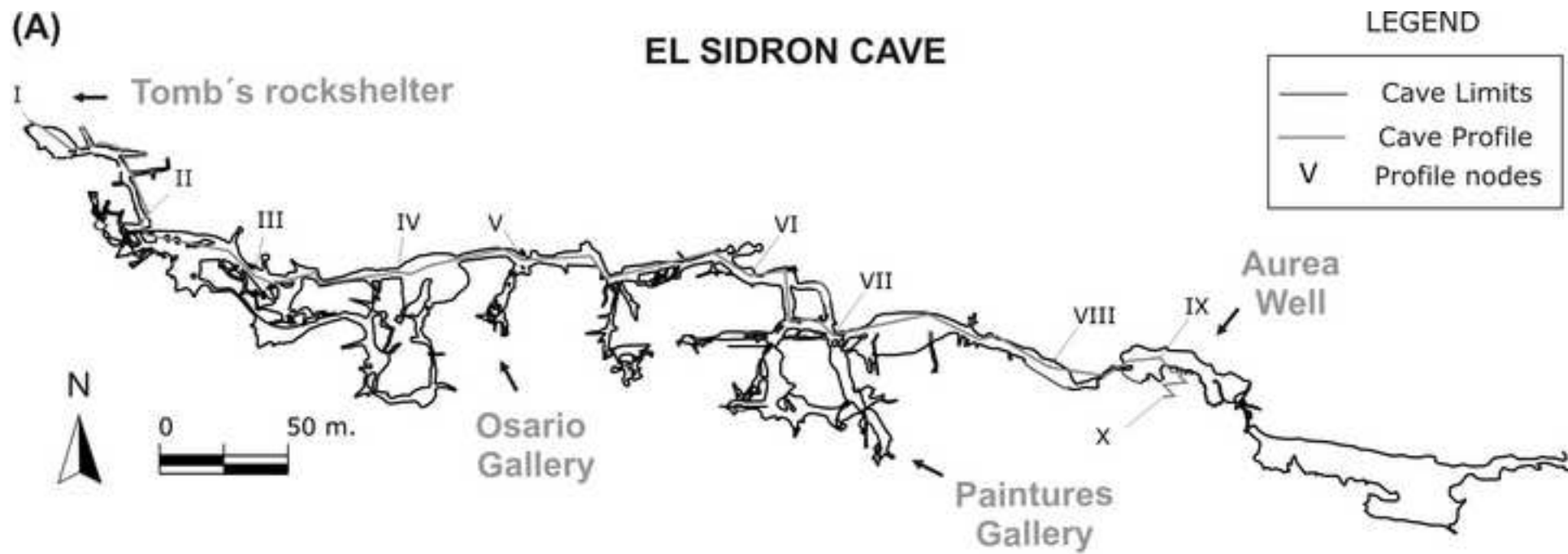


Figure 8
[Click here to download high resolution image](#)

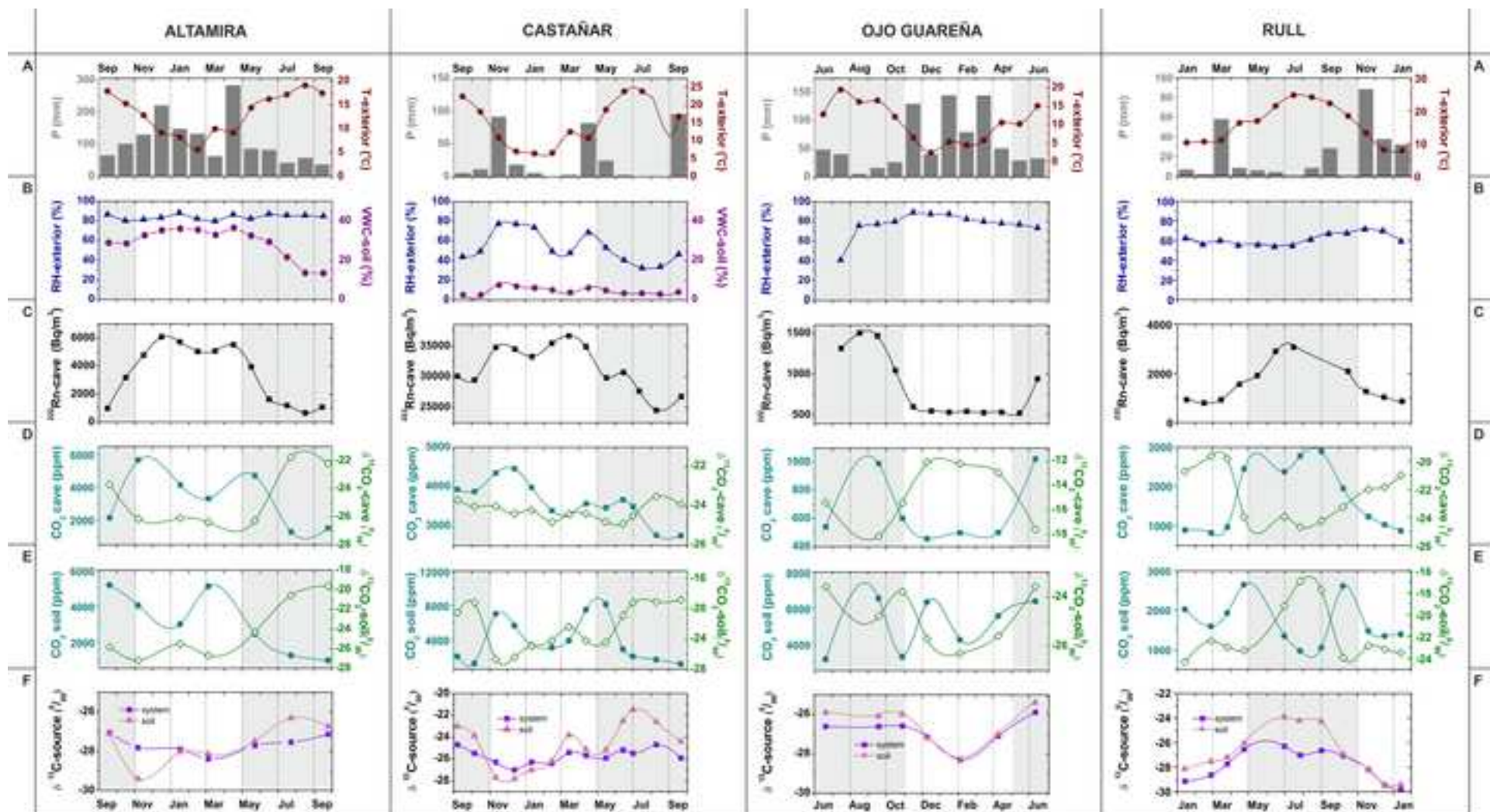


Figure 9

[Click here to download high resolution image](#)

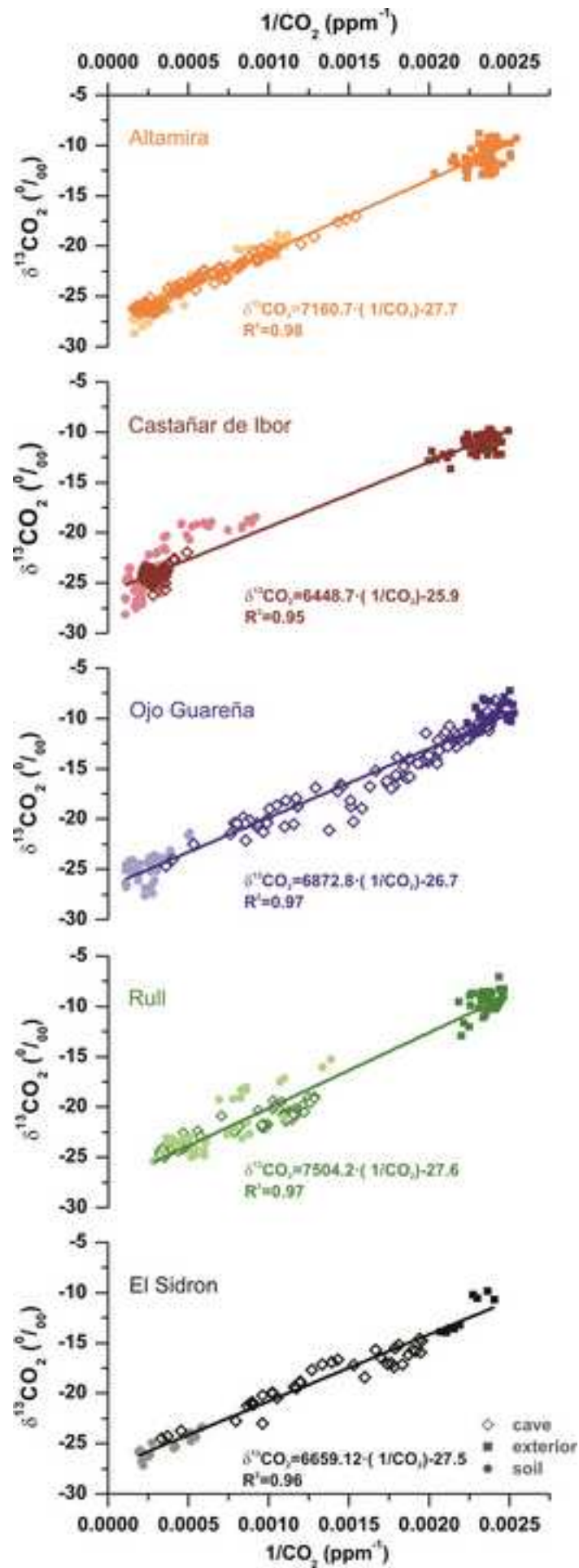


Figure 10
[Click here to download high resolution image](#)

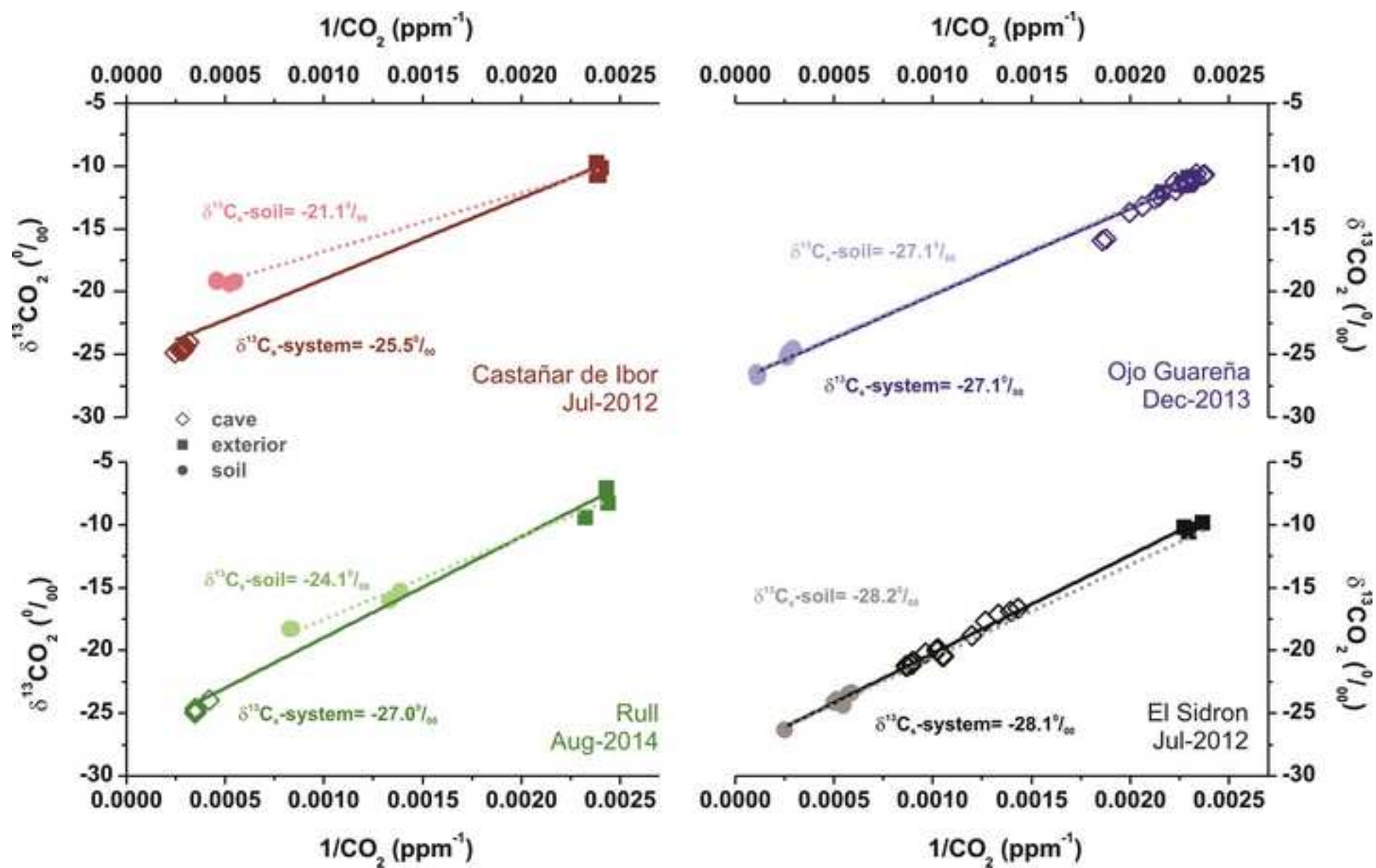


Figure 11
[Click here to download high resolution image](#)

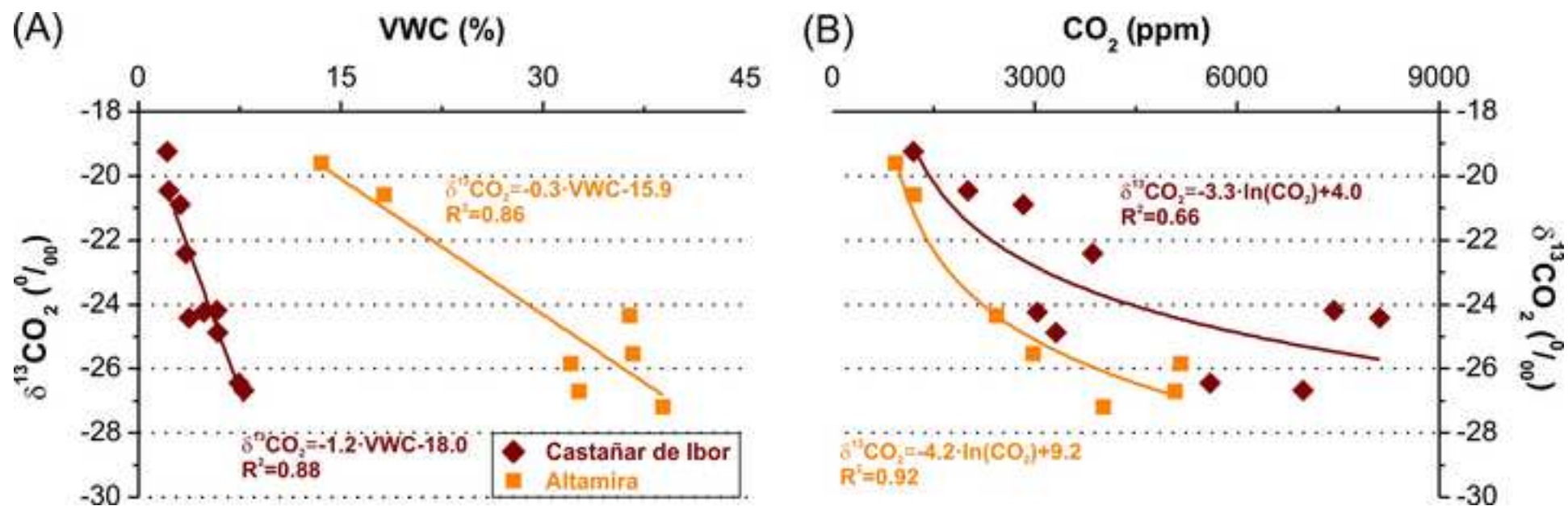


Figure 12
[Click here to download high resolution image](#)

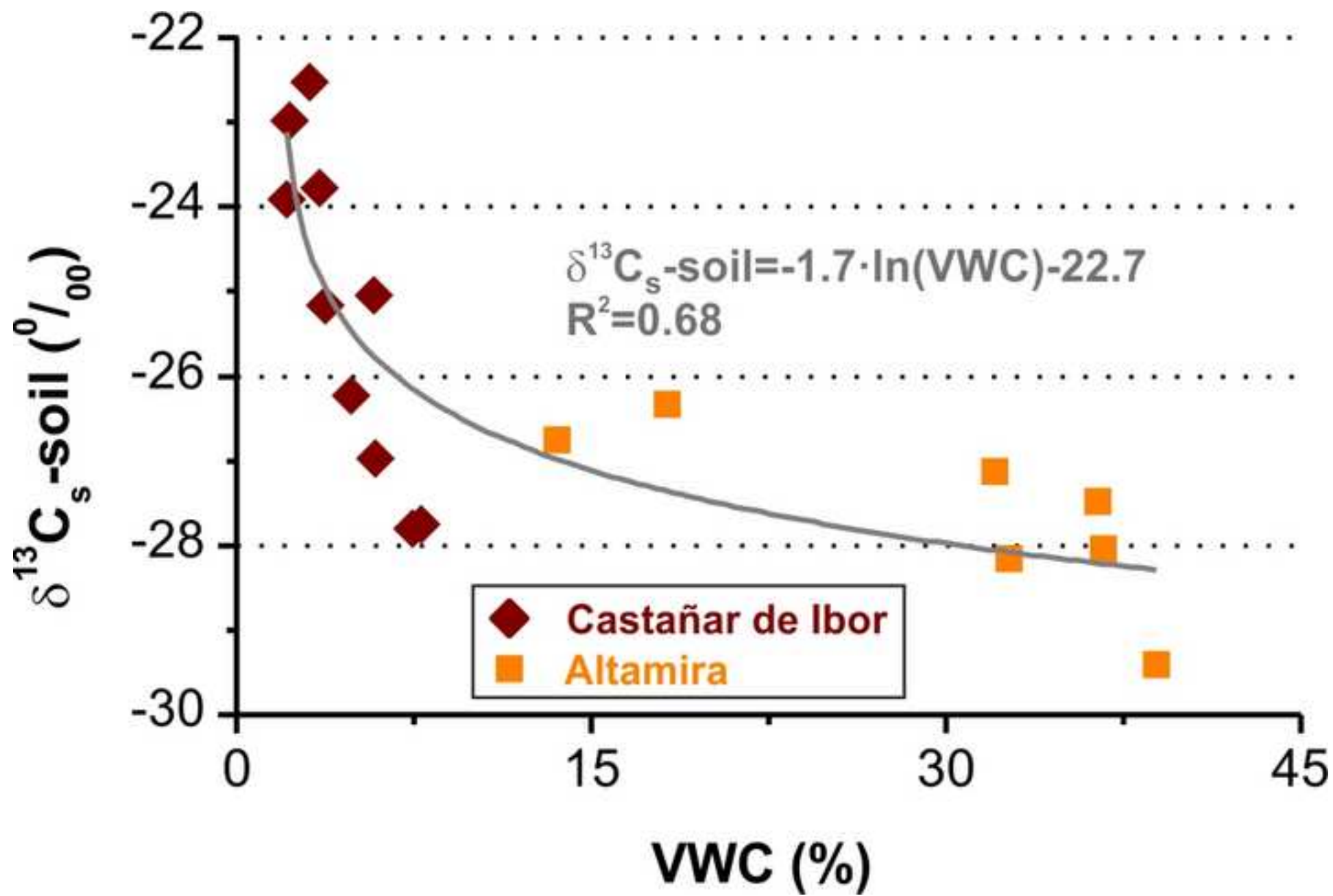


Figure 13

[Click here to download high resolution image](#)

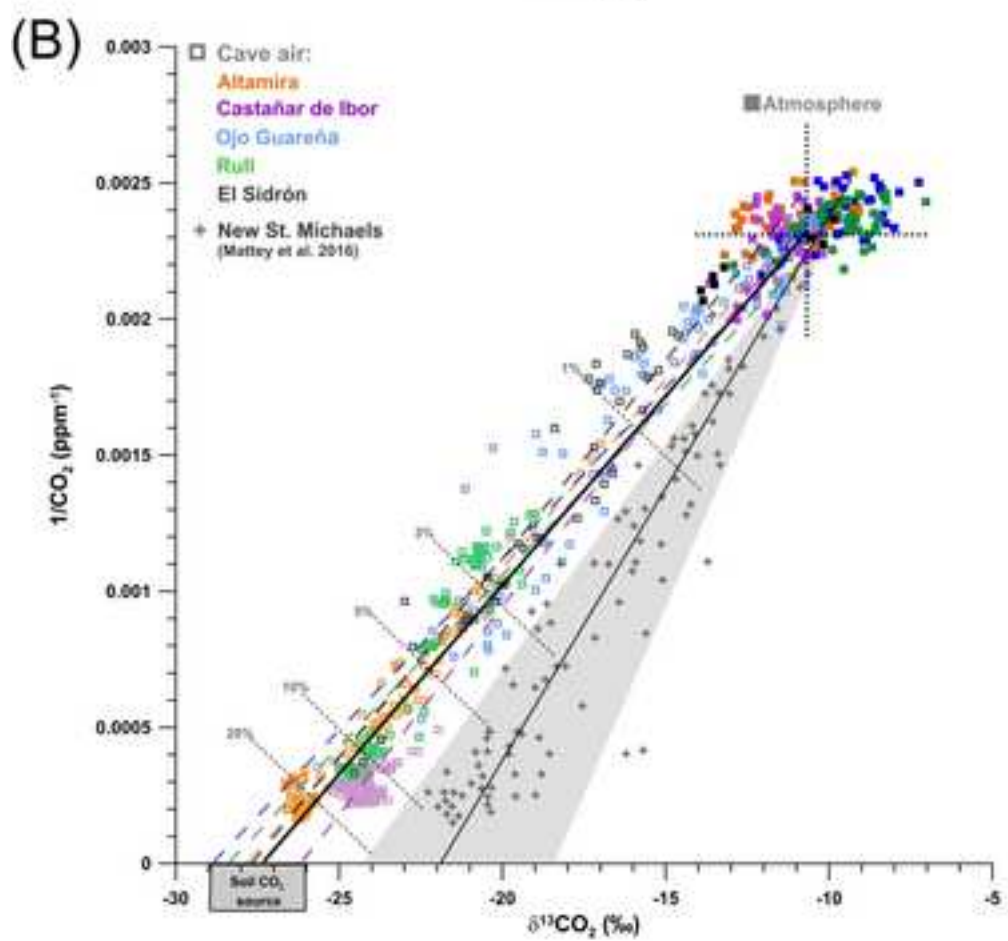
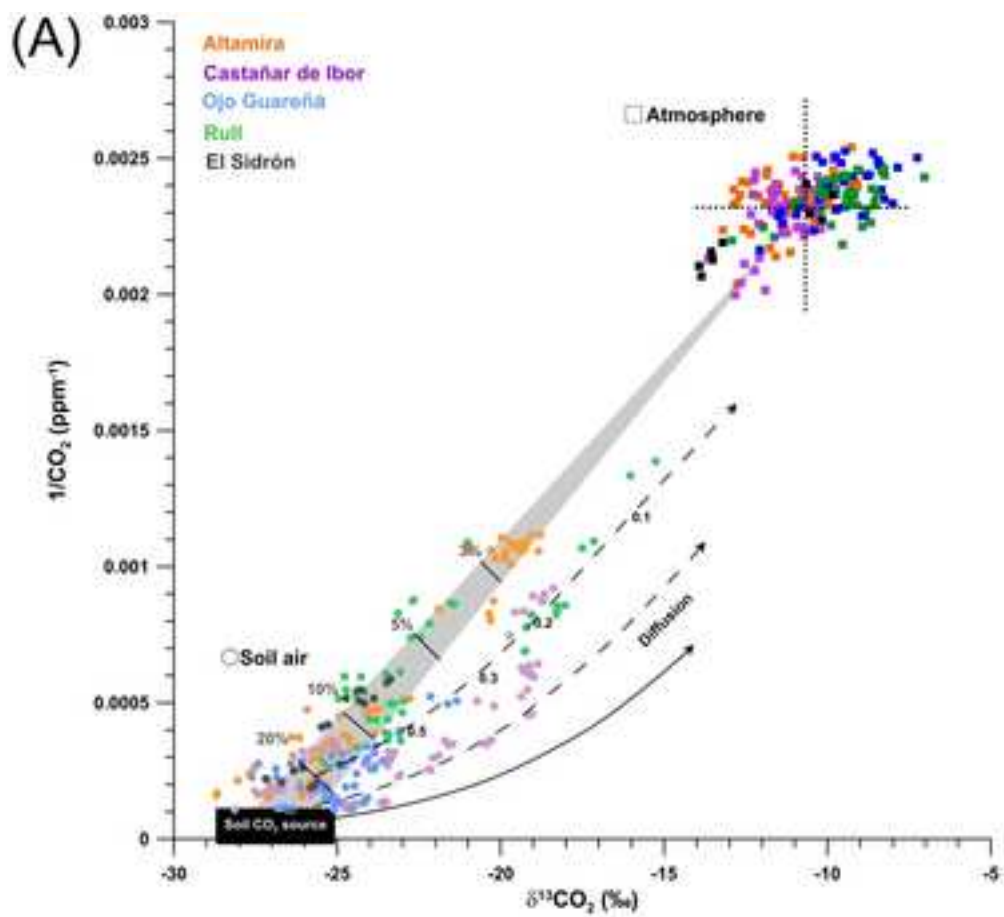


Figure 14

[Click here to download high resolution image](#)

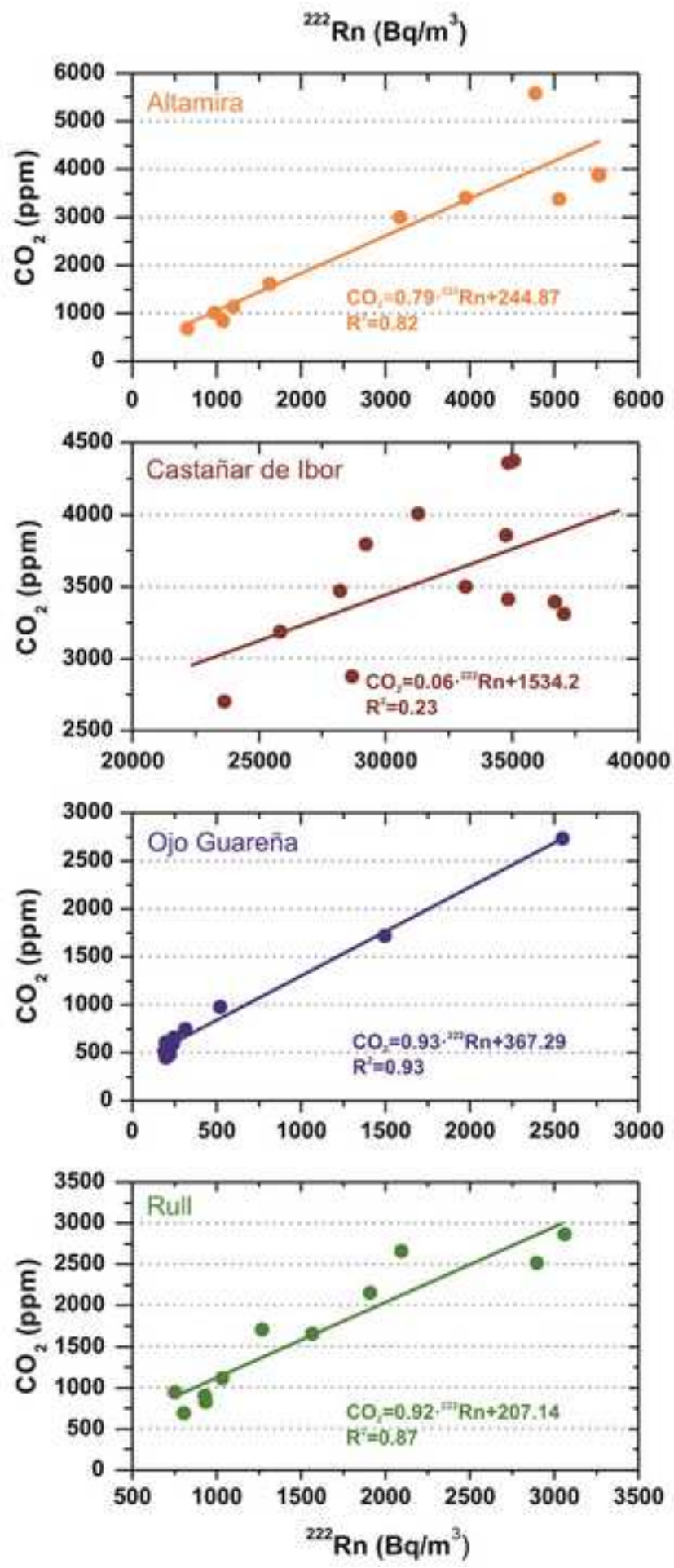


Figure 15
[Click here to download high resolution image](#)

